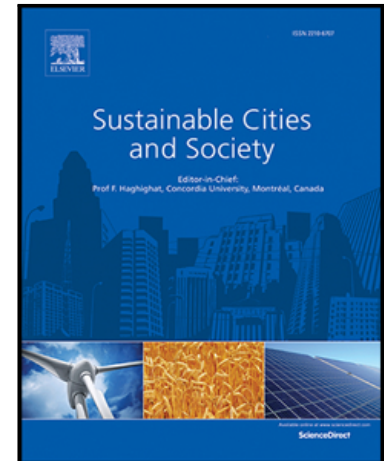Since January 2020 Elsevier has created a COVID-19 resource centre with free information in English and Mandarin on the novel coronavirus COVID-19. The COVID-19 resource centre is hosted on Elsevier Connect, the company's public news and information website.

Journal Pre-proof

Airborne and Aerosol Pathogen Transmission Modeling of Respiratory Events in Buildings: An Overview of Computational Fluid Dynamics

Yahya Sheikhnejad , Reihaneh Aghamolaei , Marzieh Fallahpour , Hamid Motamedi , Mohammad Moshfeghi , Parham A. Mirzaei , Hadi Bordbar

Please cite this article as: Yahya Sheikhnejad , Reihaneh Aghamolaei , Marzieh Fallahpour , Hamid Motamedi , Mohammad Moshfeghi , Parham A. Mirzaei , Hadi Bordbar , Airborne and Aerosol Pathogen Transmission Modeling of Respiratory Events in Buildings: An Overview of Computational Fluid Dynamics, *Sustainable Cities and Society* (2022), doi: https://doi.org/10.1016/j.scs.2022.103704

This is a PDF file of an article that has undergone enhancements after acceptance, such as the addition of a cover page and metadata, and formatting for readability, but it is not yet the definitive version of record. This version will undergo additional copyediting, typesetting and review before it is published in its final form, but we are providing this version to give early visibility of the article. Please note that, during the production process, errors may be discovered which could affect the content, and all legal disclaimers that apply to the journal pertain.

Highlights

- Challenges against CFD modeling of airborne pathogen droplets are identified

- Technical details of CFD modeling of many recent studies are summarized

- Consideration of particle dynamic phenomena in CFD models is discussed

- Experimental approaches to validate and set-up CFD models are explained

- Uncertainties in the clinical data used in CFD models are addressed in detail

Airborne and Aerosol Pathogen Transmission Modeling of Respiratory Events in Buildings: An Overview of Computational Fluid Dynamics

Yahya Sheikhnejad[1,2], Reihaneh Aghamolaei[3], Marzieh Fallahpour[3], Hamid Motamedi[4], Mohammad Moshfeghi[5], Parham A. Mirzaei[6*], Hadi Bordbar[7]

[1]Centre for Mechanical Technology and Automation, Department of Mechanical Engineering, Universidade de Aveiro, 3810-193 Aveiro, Portugal
[2] PICadvanced SA, Creative Science Park, Via do Conhecimento, Ed. Central, 3830-352 Ílhavo, Portugal.
[3]School of Mechanical and Manufacturing Engineering, Faculty of Engineering and Computing, Dublin City University, Whitehall, Dublin 9, Ireland
[4]Department of Mechanical Engineering, Tarbiat Modares University, Iran
Department of Mechanical Engineering, Sogang University, Seoul, Korea
[6] Architecture & Built Environment Department, University of Nottingham, University Park, Nottingham, UK
[7] School of Engineering, Aalto University, Finland

[*]Corresponding author: Parham.Mirzaei_Ahranjani@nottingham.ac.uk

Abstract

Pathogen droplets released from respiratory events are the primary means of dispersion and transmission of the recent pandemic of COVID-19. Computational fluid dynamics (CFD) has been widely employed as a fast, reliable, and inexpensive technique to support decision-making and envisage mitigatory protocols. Nonetheless, the airborne pathogen droplet CFD modeling encounters its limitations in the oversimplification of involved physics and the intensive computational demand. Moreover, uncertainties in the collected clinical data required to simulate airborne and aerosol transport such as droplets′ initial velocities, tempo-spatial profiles, release angle, and size distributions are broadly reported in the literature. Furthermore, there is a noticeable inconsistency around these collected data amongst many

reported studies. Hence, this study aims to review the capabilities and limitations associated with CFD modeling. Setting the CFD models needs experimental data of respiratory flows such as velocity, particle size, and number distribution. Hence, we will also briefly review the experimental techniques used to measure the characteristics of airborne pathogen droplet transmissions together with their limitations and reported uncertainties. Moreover, the relevant clinical data related to pathogen transmission needed for postprocessing of CFD data and translating them to safety measures will also be reviewed. Eventually, we scrutinize the uncertainty and inconsistency of the existing clinical data available for airborne pathogen CFD analysis to pave a pathway toward future studies ensuing these identified gaps and limitations.

Keywords: airborne pathogen; aerosol; respiratory events; CFD; buildings; droplet release; COVID19 [**Word Count**: 9,000]

Nomenclature

Parameter	unit	Explanation
C		Concentration
D		Diffusion coefficient
C_p	J/kg.K	Specific heat capacity
k_{th}	W/m. ^{o}C	Thermal conductivity
k	m^2/s^2	Turbulent kinetic energy
$\dot{m}$	kg/s	Mass flow rate (mass flux)
V	m/s	Velocity
L		Latent heat
P	Pa	Pressure
R		Universal gas constant,
T	^{o}C	Temperature
t	s	Time
M	gr/mole	Molecular weight
X		Equilibrium mole fraction of water vapor at the droplet surface
Re		Reynolds number
Sh		Sherwood number
Nu		Nusselt number
Sc		Schmidt number
y^+		Non-dimensional distance (based on local cell fluid velocity) from the wall to the first mesh node.
Greek symbols		
μ	Pa.s	Viscosity
ρ	kg/m^3	Density
ε	m^2/s^3	Dissipation rate of turbulent kinetic energy
ω	m^2/s^3	The specific rate of dissipation of turbulence kinetic energy
Subscripts		
a		air
p		particle
f		fluid

in		inlet
v		(water) vapor
∞		free stream, or fluid property at infinity
mix		mixture
s		surface
Abbreviations		
CFD		Computational Fluid Dynamics
CFL		Courant–Friedrichs–Lewy
RANS		Reynolds-averaged Navier–Stokes
LES		Large Eddy Simulation
MV		Mixing Ventilation
DV		Displacement Ventilation
UFAD		Under-floor Air Distribution
DNS		Direct Numerical Simulation
STP		Standard Temperature and Pressure (T=273.15 K and P=100 kPa)
HVAC		Heating, ventilation and air condition
WHO		World Health Organization
COVID		Corona Virus Disease
SARS		Severe Acute Respiratory Syndrome
PVT		Peak Velocity Time
CPRF		Cough Peak Flow Rate
PDA		Phase Doppler Anemometry
HSI		High Speed Imaging
LDA		Laser Doppler Anemometer
PTV		Particle Tracking Velocimetry
PIV		Particle Image Velocimetry

Table of Contents

1. Introduction

A few months after the start of the outbreak of the new epidemic virus in December 2019 in China, the world observed an extraordinary fast-growing highly contagious pandemic disease, known as COVID-19 or SARS-COV-2, which still is devastating the economics of many countries and taking many lives globally. Furthermore, arising shocks in demand and supply chains caused sustainability and management global challenges. Examples are a significant change in plastic [1] and waste management [2] or alteration in occupancy and energy demand of the building sectors [3]. This imposed a detour of many engineering disciplines, besides medicine, epidemiology, and microbiology, to redirect their attempts toward proposing feasible remedies to mitigate the spread of this highly contagious disease. In this respect, one of the key areas is aerosol science, as COVID19 was recognized to be highly transmitted via airborne droplets released from infected bio-sources [4]. In response to the development of reliable guidelines, responsible organizations such as the world health organization (WHO) have been encountered significant uncertainties in the required fundamental knowledge to be able to accurately determine how far the virus-laden airborne droplets may travel.

Although heavy released respiratory droplets deposit within less than 1-2 meters, micron-size droplets travel more up to a few meters or even become suspended for a considerably longer time, depending on the thermal effect of the bio-source, ambient humidity, and temperature, and background velocity [5,6]. Measurement techniques and experimental studies have been employed in the past decades to quantify the travel distance of deposited and airborne virus-laden particles. However, these techniques demand complex and expensive setups to observe droplets. Yet, all range of particles might not be covered due to the limitation of devices in terms of accuracy and functionality [7,8]. Besides, a major limitation has always been identified in the measurement studies in maintaining a consistent environmental condition caused by background velocity on the droplet release rate from bio-sources. In response to such limitations, computational fluid dynamics (CFD) has emerged as an in-hand, reliable, and cheap tool to study airborne pathogens released from bio-sources. High-fidelity CFD models can simulate and trace thousands of generated airborne droplets from mild to severe respiratory events, which are evaporating, colliding, or separating through their path as they may linger within indoor environments. Despite the cheaper and faster advantage of implementing high-fidelity CFD models, these models encounter three significant limitations, including (1) computational costs, (2) uncertainty in the collected clinical data needed for setting CFD models, (3) and oversimplification of the underlying physics.

In terms of computational cost, the nature of a transient 3D motion of two-phase turbulent flow requires fine meshes (a cluster of control volumes) while simulations should be conducted with short time-steps to capture high gradients and small-scale phenomena including particle breakup, collision, and evaporation. Taking all these details into account requires an extremely high number of cells causing slow simulation speed. In other words, a well-organized CFD model is highly time-consuming and computationally expensive, which can consequently demand enormous computational resources such as supercomputers and clusters.

Moreover, airborne pathogen droplet CFD models demand a series of complex clinical datasets as inputs, which were solely gathered in this respect before the current pandemic. Most of the clinical data were measured experimentally. However, as reviewed in section 6, the available clinical data are inconsistent in terms of variations and level of uncertainties. This diversity and uncertainties may be due to the instrumentation uncertainties and limitations, inevitable human errors, and neglecting the effect of important parameters, which are also discussed in this paper.

Regarding oversimplification of the underlying physics, many fundamental understandings such as Brownian and turbulent motions are yet weakly represented in the available models. Each turbulent model is tailored for a branch of applications and has several tuning parameters that have to be set properly [9]. However, such models are yet to be improved and calibrated for applying submicron airborne pathogen droplet CFD modeling. The discussed limitations may influence the advantage of CFD models and devaluate their results. Hence, understanding the weaknesses and strengths of the currently available clinical data for being used as an initial and boundary conditions in CFD simulations and avoiding the development of oversimplified models is essential.

In this respect, this study paves the path for future numerical studies by providing comprehensive data required for CFD modeling of airborne and aerosol transmission from respiratory events. The limitation related to the computational cost is not discussed in this study as the available technical data was not found to be sufficient to help to draw solid conclusions. Related to two other limitations, more than 130 related peer-reviewed scientific papers were addressed to present the most agreed data in the corresponding scientific communities. As the first step, this manuscript intends to provide an overview of the definition of common jargons related to the transmission and dispersion of airborne pathogen droplets from respiratory events, which are frequently used in literature as presented in Section 2. In Section 3, this paper scrutinizes the related abilities of airborne pathogen droplet CFD modeling (see Fig. 1) in enclosed spaces (i.e., hospitals, public transportations, schools, offices, and residential buildings). It further addresses the CFD modeling of airborne pathogen and related settings for numerical simulation as presented in Section 4. Experimental approaches, which are essential for both

validation and supplying input data for CFD models, are described in Section 5, while the associated drawbacks are discussed. Eventually, the clinically reported input datasets, focusing on their strengths and weaknesses, are presented in Section 6.
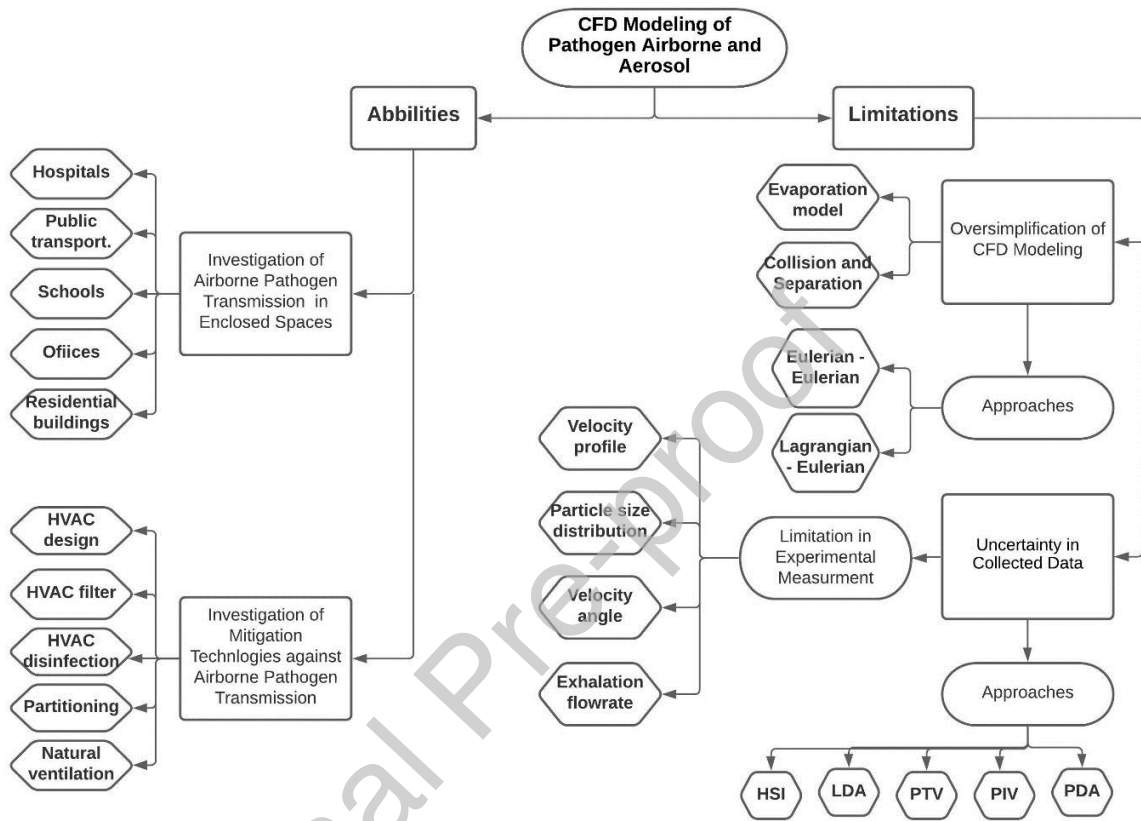
Fig. 1: The schematic of the capabilities and limitations of airborne and aerosol pathogen CFD modeling.

2. Terminologies

The complex nature of COVID-19 transmission and the catastrophic consequences of its pandemic require scientists from various disciplines such as fluid dynamics, aerosol physics, behavioral psychology, epidemiology, virology, public health, and public policy to work together while their technical terminology may not essentially concord. The contradiction exists in definitions of some interdisciplinary terms such as airborne and aerosol in publications of different fields, which can cause misunderstandings or even disconnections between research findings of various fields. Hence, in this section, some of the main terms used in this paper are defined. Nonetheless, the given terminologies are more in line with those used by the fluid dynamics research community.

- *Large droplets* refer to respiratory droplets with the size of 50μm or larger, which mostly follow the ballistic trajectory and, hence, settle down on surfaces at a distance from the bio-source.

- *Small droplets* refer to droplets smaller than 50 μm, which undergo fast evaporation and convert to aerosol.

- *Airborne* describes particles of any size and can be infectious particles, pathogen-containing, small droplets, and particles suspended in the air over a long time and carried over by air mainly as suspended particles [10].

- *Aerosol* refers to particles with tiny size lingering with the background flow. They can be a suspension of fast-drying liquid droplets, droplet nuclei, or particles in the air [5]. They can contain infectious pathogens, mucus, water, salt, etc.

- *Background flow* refers to the flow field, encompassing the jet generated by a bio-source mainly disturbed by ventilation, environmental temperature and relative humidity, and movement of bio-sources.

- *Respiratory events* include breathing, speaking, singing, coughing, and sneezing.

- *Reynolds number* definition may vary based on a situation and application, e.g., for an internal flow. It can be defined as $Re = \frac{\rho_f \bar{V}_{in} D_h}{\mu_f}$, where D_h and $\bar{V}_{in}$ are the hydraulic diameter and average fluid velocity at the inlet section, respectively, while for calculations of the drag force in a continuum media and over a particle, it can be defined as $Re = \frac{\rho_f \bar{V}_{p,rel} D_p}{\mu_f}$, where D_p and $\bar{V}_{p,rel}$ are the particles' diameter and relative velocity, respectively.

- *Stokes number* (St= $u_0 t_0 / l_0$) indicates the ratio of the characteristic time of a particle (or droplet) to a characteristic time of the flow or of an obstacle. Here, u_0 is the fluid velocity of the flow well away from the particle, t_0 is the time constant in the exponential decay of the particle velocity due to drag (the relaxation time of the particle), and l_0 is the characteristic dimension of the particle (typically its diameter).

3. Airborne Pathogen CFD Modeling in Enclosed Spaces

As a part of a sustainable solution and achieving resilience against a hostile guest, the major core of our infrastructures, such as hospitals, public transportation, schools, offices, and residential buildings, have to be reinforced by a suitable design. In addition to health-related benefits, the infection spread as a major global issue imposes undesirable social and economic costs through absenteeism, lost productivity, costs of medical treatment, and a high rate of mortality [11]. By simulating a global economic model though G-cubed model which is a hybrid of dynamic stochastic general equilibrium models and computable general equilibrium models, it is found that such considerations are more urgent since the consequences of COVID-19 could have a considerable impact on world economics, more that it is expected [12]. In this regard, understanding principles of respiratory infection transmission, aerosol

and droplet deposition, and dilution, as well as implications of background airflow, are critical in providing recommendations and principled measures at the community and organizational level during contagious airborne pandemic diseases [13].

COVID-19 transport in enclosed spaces has been studied in different types of buildings such as hospitals [14–23], public transportation [24–26], schools [27,28], offices [29,30], and residential buildings [31,32]. Reviewing the literature reveals that the background airflow pattern is a pivotal factor in airborne disease transmission, which is highly affected by different parameters related to (1) space (e.g., geometry and layout, usage type, equipment and furniture, and infiltration rate from cracks and voids), (2) HVAC (e.g., type of ventilation system, supply air parameters), (3) occupant (e.g., respiration performance, activity type such as walking, sitting or other types of activities [11,33]. Therefore, the design of indoor conditions can benefit from respiratory airborne and aerosol transmission modeling to analyze or optimize engineering solutions [34–41]. In this regard, several solutions have been practiced on mitigation of airborne pathogen transmission such as HVAC control [42,43], HVAC-design [44,45,54,46–53], HVAC-filter [55–60], HVAC-disinfection [16,61,70–73,62–69], partitioning [35,74,75], natural ventilation [57,76–80], and personal protective equipment (PPE) [81–88].

In some of these studies, the efficiency of the used methods was investigated in accordance with the location of infection sources/patients and as a result, detailed guidelines were suggested for indoor spaces. For instance, [14] showed that virus particles would deposit mainly back on the source patient and as such, if the patient is close to the hallways, the virus particles would be exhausted to the corridor while if patients were in the inner parts of rooms, the virus particles would probably deposit on the wall surfaces. Such studies show that investigating the impact of HVAC design and other technical solutions should be tailored to the internal layout of infection source as the existing condition while there should be flexibilities in possible future changes in buildings' layouts. This issue is more critical in hospital wards as one of the most complicated scenarios with different infection sources in enclosed spaces [14,15,49].

With this understood, CFD modeling has already been employed to provide solutions against many of the arisen challenges. Nonetheless, its potential to support many remedial technologies is yet to be explored in the near future as a trend toward this need can be evidently observed from the recent studies. In this regard, a brief overview of CFD technical details employed in previous studies with important insights is presented in Table 1. These studies are summarized in different groups of HVAC-design [14,18,54,60,89,19,20,23,29,33,51–53], HVAC-disinfection [62,71,73], natural ventilation [31,80], partitioning [75] and PPE [87,88]. In the HVACdesign as the most common theme, the impact of various HVAC strategies such as mixing ventilation (MV), displacement ventilation (DV), and under-

floor air distribution (UFAD) on particle dispersion has been widely studied [44,45,54,46–53]. Also, applications of specific parts of HVAC systems such as filters are reviewed in the section [55–60].

As highlighted in Table 1, the modeling approach, geometry of spaces, turbulence model, and accurate flow-thermal boundary conditions are essential factors to implement the CFD modeling of airborne and aerosol pathogen transmission. The most important boundary conditions for respiratory events are flow rate and jet direction, temperature and size distribution of the virus droplets [90–92]. The airflow pattern and virus dispersion modelling are mostly studied in previous papers to investigate the impact of HVAC systems, as a remedial technology, which are mainly solved within Eulerian-Lagrangian frameworks. These features of boundary conditions significantly change the performance of numerical models, which emphasize the need to develop detailed frameworks tailored for each case study that can vary from a hospital ward, or office to a ventilation duct to ensure the accuracy of the model. Direct Numerical Simulation (DNS), Large Eddy Simulation (LES) and Reynolds-Averaged Navier-Stokes (RANS) are three main applied turbulence models in which the RANS models are more applicable and preferable to simulate airborne infection problems [49,52]. One of the main reasons is due to the fact that the RANS method generally requires less computation capacity while providing an acceptable accuracy and reliability level [53,93]. Also, among the RANS turbulence models, the RNG k-ε model is tested and validated to be an appropriate choice [14,29,94,95] as it can provide better accuracy and stability in terms of low Reynolds number and near-wall flows [14,53]. Furthermore, in some studies presented in Table 1, the airflow condition is assumed isothermal [19,20,51,52,62]. This assumption is mostly observed in studies that have a relatively small spatial domain to analyze while the investigation is mainly considered for sneezing and coughing, where particles are released at a high rate and the buoyancy effect is less effective [20].

Table 1- Overview of technical details of airborne pathogen droplet CFD modelling in enclosed spaces.

Ref.	Remedial Technology	Research approach	Turbulence model	Droplet treatment	Boundary Condition	Validation	Geometry description	Background flow	Key findings
[14]	**HVAC-design**	Airflow field and virus dispersion modelling within	RNG k-ε	Coughed droplets size of	**Wall:** Adiabatic boundary type at the building walls - Heat flux at the human bodies **Inlet-mouth:**	-	Six-bed general ward cubicle with 7.5 m (L) ×	Yes	Location of a patient and the air exchange rate in

		Eulerian-Lagrangian framework to solve the gas-solid two-phase flow problem	8.3μm - Density of 1,100 kg/m^3	exhalation velocity of 50m/s **Inlet:** Specified airflow rate at four ceiling air inlets **Others:** Four-way spread-type, adiabatic and reflect boundary type at diffusers - Pressure-outlet, and adiabatic boundary type at corridor.		6 m (W) × 2.7 m (H) – 1,143,766 cells	each ward can alter the risk of transmission of viruses.
[18]	**HVAC-design**	The impact of variable air volume (VAV) primary air system on the dispersion of infectious aerosols by CFD approach based on finite element method (FEM)	RNG k-ε	Droplet diameter of 2.5 - 200μm – Cough flow rate: 5 L/s – Density: 2.5μg/dm^3 - 0.3s for the duration of a single cough	**Wall:** Constant heat transfer coefficient at all building walls **Inlet-mouth:** Cough velocity of 12m/s - Temperature: 35℃ **Inlet:** Velocity inlet at seven inlet grids of HVAC	Comparing airflow and particle concentration with experimental data	A cardiac intensive care unit room with 13.0 (L) m × 6.8 m (W) × 2.8 m (H) – 10 million cells	Yes	Wider recirculation zones can be created by high turbulence of inlet grids, combined with the air outlet grids. An HVAC system can lead to the distribution of infectious droplets on both directly exposed surfaces and less exposed or hidden areas.
[19]	**HVAC-design**	Airborne infections transmission study using particle tracking	Standard k-ε	Droplet size of 1μm	**Wall:** Adiabatic boundary type **Inlet:** Velocity inlet at two inlet grids	Comparison of air flow pattern with experimental	ICU room 6.3 (L) m × 5.8 m (W) × 3.0 m (H) –	Yes	The importance of outlet position for transferring

	module					data	385,000 Tetrahedral unstructured cells	contaminant particles is highlighted in hospitals.
[20]	**HVAC-design**	Simulate the transport of droplets and bioaerosols for design optimization of local exhaust ventilation	Standard k-ε	Three particle sizes of 1, 10, and 50 µm in diameter	**Wall:** Adiabatic boundary type **Inlet-mouth:** Sneezing velocity of 100m/s	Comparison of airflow and aerosol concentration with experimental data	A single patient room 6.7 (L) m × 6.0 m (W) × 2.7 m (H) – 1.6 million tetrahedral unstructured cells	No	Local exhaust ventilation is a promising strategy to remove the contagious pollutants for health care workers who need to be in close contact with patients.
[51]	**HVAC-design**	Particle dispersion and deposition modelling with a drift-flux model (one of the simplified Eulerian methods) for three typical air distribution systems (MV, DV, and UFAD)	Standard k-ε	Droplet diameter of 1 - 20µm - Density of 1,000kg/m³	**Wall:** Adiabatic wall at the floor, ceiling, and walls - Uniform heat flux at window - Constant temperatures at human body **Inlet-mouth:** Steady inhalation, respiration rate of 8:4 l min⁻¹ - Turbulence intensity: 20% **Inlet:** Uniform airflow rate at MV, DV and UFAD inlet	Comparison of particle concentrations with experimental data of other studies	A hypothetic room with 4.0 (L) m × 3.0 m (W) × 2.7 m (H)	Yes	DV and UFAD systems have better performance to reduce exposure risk, especially for super-micron particles.

[52]	**HVAC-design**	Lagrangian method of CFD simulation to evaluate the spatial distribution and temporal of coughed droplets	RNG k-ε	Coughed droplets size: 10μm - Total flow rate: 2.4e⁻⁹ kg/s – Density: 1,000kg/m³ - 1s for the duration of a single cough	**Wall:** Adiabatic wall at the building's walls - Uniform heat flux at the human bodies **Inlet-mouth:** Velocity of 10m/s **Inlet:** Velocity inlet at MV and DV supply air	-	The air-conditioning room with 4.0 (L) m × 5.0 m (W) × 3.0 m (H) and with two people standing face to face	Yes	Preceding 5s, the main factors that affect coughed droplets distribution are the initial conditions of expelled air, while after 5s the indoor airflow is the main factor.
[53]	**HVAC-design**	CFD simulation to analyze the spatial concentration distribution and particle tracks of students talking continuously	RNG k-ε	Droplet size: 5μm - Total flow rate: 0.085 μm/s – Density: 600kg/m³	**Wall:** Adiabatic wall at the building's walls – Uniform temperature at the human bodies **Inlet-mouth:** Initial velocity: 1m/s – Temperature: 308K **Inlet:** Velocity inlet at the MV and DV inlet	-	A classroom occupied by 10 students with a seating arrangement of 5 rows and 2 columns	Yes	DV systems with low air supply velocity and low turbulence have more efficiency in removing the respiratory aerosol droplets and minimizing the risk of infection.
[54]	**HVAC-desig**	CFD simulation to optimize	Standard k-ε		**Wall:** constant heat source of 70W at the human	Comparison of velocit	An isolation room	Yes	Immune-suppressed patients

]	n	the ventilation strategy towards contaminant suppression			bodies **Inlet:** Inlet velocity at air supply openings	y distribution at various locations inside chamber with experimental data of other studies	with 4.88 (L) m × 3.60 m (W) × 3.05 m (H) with bed and body of the patient – Unstructured tetrahedral cells with fine mesh near the patient body (0.01 m) and coarse towards the isolation room walls (0.2 m).		should be placed next to the air supply and infectious patients near the exhaust.
[23]	**HVAC-design**	CFD-based numerical model integrated with the Wells-Riley equation to assess risk of airborne infection	Standard k-ε	Droplet size of 5μm	**Wall:** Constant temperature at body surfaces, windows and doors - Adiabatic condition at other walls **Inlet-mouth:** Initial velocity of 1.87m/s for driver, 1.07 m/s for other people- Temperature: 20.2 ℃ when inhalation and 34 ℃ when exhalation **Inlet:** Velocity inlet at air supply opening **Outflow:** opening - Free-slip at air exhaust opening	-	A bus cabin with different occupancy scenarios - 120 million tetrahedral spatial cells and 200,000 triangular surface meshes	Yes	The DV method is more effective in limiting the risk of airborne infection in public buses. Air distribution method, location of return/exhaust opening, and seat arrangement change the performan

									ce of mixing ventilation methods in buses.
[29]	**HVAC-design**	Transmission of respiratory droplets between two seated occupants within Eulerian method (drift-flux model)	RNG k-ε	Droplet size: 0.8 μm, 5 μm, 16 μm - Density – 1,000 kg/m³,	**Wall:** Constant heat-flux at human bodies **Inlet-mouth:** Exhaled infected airflow: 6 min⁻¹ - Temperature: 35 ℃ **Inlet:** Velocity inlet at the supply air **Outflow:** Free-slip at air exhaust opening	Comparisons of simulated and experimental particle concentrations	A single room 5.4 (L) m × 4.80 m (W) × 2.6 m (H) containing two people – Combination of unstructured tetrahedral mesh and hexahedral mesh with 994,634 cells	Yes	Personalized ventilation devices for seated occupants in offices can increase the average concentration in the occupied zone of the exposed individual and provide clean personalized airflow.
[33]	**HVAC-design**	Distribution of droplet aerosols evaluation in an air-conditioned room with Lagrangian method	LES	The initial droplet size: 1, 10, 20, 50 and 100 μm - Density – 998.2 kg/m³,	**Wall:** Different heat-flux at height of human bodies - Adiabatic condition at other walls **Inlet-mouth:** Exhaled infected airflow: 100 s⁻¹ - Temperature: 35 ℃ - RH: 90% **Inlet:** Reflect type and Velocity inlet **Outflow:** Escape type	Comparison of droplet distribution with experimental data	The full-scale room with 8.74 (L) m × 4.95 m (W) × 3.63 m (H), containing 16 diffusers and a woman – 2.6 million unstructured cells	Yes	The influence of supply air temperature and relative humidity on the number of the suspected droplets is less than ventilation rate and air distribution patterns in DV system.
[	**HVA**	Transmissi	Reali	Drop	**Wall:** Constant	Compa	A	Yes	The case,

[89]	**C-design**	on of respiratory droplets and optimization of ventilation systems to control the spread of airborne particles in a classroom with Lagrangian method	zable k-ε	let size: 1.25 µm	heat-flux at body surfaces **Inlet-mouth:** Initial velocity of 0.2m/s - Temperature: 34 ℃ - Total flow rate: $1.25 \times e^{-5}$ kg/s **Inlet:** Velocity inlet	rison of infection concentration at various positions with experimental data of other studies	classroom with 9.77 (L) m × 7.25 m (W) × 3 m (H) occupied by 30 students with a seating arrangement of 5 lines and 6 rows – 23.6 million unstructured cells		including the inlets and outlets, separately, on the floor and ceiling of each student, has the better performance to minimize the infection spreading since the maximum value of residential time of infections is 4s in the case study.
[60]	**HVAC-design**	CFD simulation based on the Lagrangian discrete particle tracking to simulate the behavior of fibrous filters used to treat aerosols	Coupling of the customized particle solver with the volume-of-fluid (VOF) solver as the new solve	Particle diameters of 50–1,000 nm – Particle velocity of 0.1m/s.	-	Validation of each solvent component accurately and sequentially against known analytical or experimental relationships such as particle physics or plate-rail	4 fibres in a grid pattern with 10 µm diameter, situated in a cube with 100 µm × 100 µm × 100 µm - A series of meshes with cell sizes ranging from 1.667 to 5 µm	No	The time-step size and cell volume are important factors in simulating aerosols using Lagrangian modelling.

		r			instability		

[62]	**HVAC-disinfection**	CFD simulation based on the Discrete Phase Modeling (DPM) and Discrete Ordinates (DO) radiation modelling to analyze Ultraviolet (UV) dose values, distributions, and disinfection rate in different lamp arrays of an in-duct Ultraviolet-C (UVC) system	Standard k-ε	Particle average diameter: 1 µm – Density: 1,000 kg/m^3	**Wall:** Adiabatic condition in the system - Semi-transparent and a diffuse fraction of 1 at the lamps - Diffuse wall reflectivity of 15% at the inner surfaces of the duct **Inlet:** Velocity inlet and injection surface at air supply inlet of the duct	-	A ventilation duct with 7.83 (L) m × 0.61 m (W) × 0.61 m (H) containing four identical UV lamps with a diameter of 1.90 cm and length of 53.82 cm distributed with four lamp array configurations – A 256k structured hexahedral mesh
[71]	**HVAC-disinfection**	CFD simulation to analyze Average UV dose and dose distribution with different UV lamp placement and	Standard k-ε	-	**Wall:** Adiabatic condition at building walls **Inlet:** Velocity inlet at air supply opening with the total flow rate of 0.0533 m^3/s **Outflow:** A static pressure boundary condition at the exhaust	-	A room with 4.26 (L) m × 3.35 m (W) × 2.26 m (H) contain UV fittings mounted on four

Note: The "No"/"Yes" column and the final description column appear as additional columns:

Ref							Config		Description
[62]							No		Changing the lamp array configuration and position remarkably alters the velocity and irradiance distributions. A horizontal configuration of the lamp array provides the most UV dose distribution over the pathogenic particles.
[71]							Yes		A ventilation system with a low-level supply and a high-level extract causes a higher average

		ventilation system				walls – 500,000 unstructured tetrahedral cells	UV dose in the room's active region than a ventilation system with a high-level supply and a low-level extract. The lamp location is critical to UV disinfection effectiveness.
[73]	**HVAC-disinfection**	CFD simulation to analyze the disinfection performance of electrostatic disinfector by Lagrangian-based integrated model	-	-	**Inlet:** Uniform Velocity inlet of 0.1 m/s type in COMSOL **Outflow:** Pressure outlet COMSOL	The experimental disinfection data from literature was adopted to validate the numerical model	two ducts with 6 m (L) × 0.1 m (H) and with the radius of discharge wire of 0.1 mm and 5 m (L) × 0.067 m (H) with the radius of discharge wire of 0.1 mm	No	For electrostatic disinfectors, applied voltage, average electric field strength and inlet velocity significantly influenced disinfection efficiency. The applied voltage is an essential controllable variable in HVAC operations.

[75]	**Partitioning**	CFD simulation to analyze the airflow pattern and airborne pathogen dispersion with installing partitions	Realizable k-ε	-	**Wall:** Constant temperature at walls **Inlet-mouth:** Average exhalation velocity of 0.2 m/s – Temperature: 36.5℃ **Inlet:** Velocity inlet at inlet **Outflow:** Split ratio outlet for outlet condition	-	A room with ten beds without and with partitions between the beds) with different diffuser locations – 2,405,265 polyhedral cells	Yes	Installing partitions can reduce average infectious airborne concentration in the room while increasing the beds around to the pathogen source.
[31]	**Natural ventilation**	Eulerian and Lagrangian approaches are adopted to investigate the dispersion of expiratory aerosols between two vertically flats	RNG k- ε	Particle size of 1, 10, and 20 μm without an initial velocity - Flow rate: 8mg/s – Density: 1,000kg/m³	**Wall:** Constant temperature at indoor wall surfaces **Inlet:** Velocity inlet at the domain inlet **Outflow:** opening - Free-slip at air exhaust opening	Comparison of the measured and simulated particle concentrations at the centre of the plane.	A four-story building with 3.1 (L) m × 2.4 m (W) × 2.7 m (H) in each story	Yes	The airflow exhausted from windows of a lower floor can be directed by wind-driven or buoyancy forces toward windows of upper floors' neighbours. The concertation rate of particles is two to three times lower in the upper levels compared to the source level.

Ref	Category	Description	Turbulence model	Particle params	Boundary conditions	Validation	Geometry		Results
[80]	**Natural ventilation**	A Eulerian-Lagrangian CFD model of exhaled droplets is developed for an office case study impacted by different ventilation strategies	Realizable $k-\varepsilon$	Particle size 2-1,000 μm– Flow rate: 4L/s	**Wall:** Adiabatic condition at walls **Room Inlet**: Temperature: 25 ℃, relative humidity: 50%	Validated with an office case study impacted by different ventilation strategies	A small office with dimensions of 4m (L) × 4m (W) × 3.2 m (H)	No	The single ventilation strategy has the highest infection probability while this strategy and no-ventilation result in higher dispersions of airborne pathogens inside the room.
[87]	**PPE**	CFD evaluation of velocity vectors and distribution of ejection during respiratory events with and without a mask	RNG k-ε	Particle size of 1-500 μm– Flow rate: 6L/s	**Inlet-mouth:** velocity of 50m/s at 0.1s	Compatibility of results with experimental data of other studies	A human face with a mouth of 2 cm^2 and a mask covering 22% of the face area around the nose and mouth	No	A simple cotton mask with a pore size ≈ 4 microns is highly effective in reducing jet's propagation. About 12% of the airflow leaks through 1 mm gap around and between the face and the mask.
[88]	**PPE**	Evaluation of droplet transmission mechanism	LES	Density: 998 kg/m^3	**Inlet-mouth:** Respiratory airflow velocity of 6.3 and 22.3 m/s-	-	The air-conditioning room with 4.0	Yes	Contamination area can be reduced to one-third

s with coupled Eulerian–Lagrangian method	Temperature: 34 ℃ **Inlet:** Velocity inlet at air conditioner inlet and window **Outflow:** Outlet pressure at the exhaust door	m (L) × 3.0 m (W) × 3.0 m (H) and with two people standing - 5.1 million unstructured cells.	and three-quarters by wearing a face mask and bending the head, respectively, during a sneeze.

4. CFD Modeling of Airborne Pathogen Droplets

4.1. Numerical approach

Modeling the dispersion of respiratory droplets and pathogens released by respiratory events (i.e., breathing, coughing, and sneezing), although having different shapes, sizes, and bio-effects, all fall into the multiphase simulation (see Appendix I for equations). Whether a Lagrangian approach should be selected or an Eulerian has always been a challenging question in the CFD modeling of respiratory events [96]. Lagrangian frameworks are utilized for particular problems related to the transport of pathogen droplets, such as the residence time (suspension time), evaporation, and deposition of large respiratory droplets [97]. Furthermore, particle tracking inside the lungs is also more simulated using Lagrangian models since the sticking of inhaled particles to the inner walls of lungs and release of particles from an unhealthy trachea can be simulated if required [98−100]. On the other hand, specific problems about respiratory effects are easier if formulated in the Eulerian framework. For example, the spread of infectious particles or toxic gases, as a continuous mixture, can be simulated via Eulerian models, which are faster than Lagrangian ones. Another group of Eulerian problems includes the thermal effects of heating and ventilation systems [101] on the spread of gaseous phases inside enclosed areas such as hospitals, as discussed in Section 3. A comparison performed by Zhang and Chen [102] in a closed space concluded that both methods could predict the steady-state concentration, while the Lagrangian method demands more computational resources. Their results also showed that the Lagrangian model is better in predicting transient dispersion of the particles. In addition, for the CFD simulation of pathogens and volatile droplets generated by respiratory events, one should consider that numerical simulation of evaporation of smaller particles (sub-moicron particles) demand smaller time-step values which add to computational costs [103]. This is contrary to the Eulerian framework, which does not include simulation of particles and hence is faster and cheaper, however, provides fewer details.

Another factor that identifies the condition of airborne droplets' transport is the Stokes number. A particle with low Stokes number follows fluid streamlines (perfect advection). In contrast, a particle with a large Stokes number is dominated by its inertia and continues along its initial trajectory. Cohen and Asgharian [104] showed that the inertial effects influence the particle deposition at Stokes numbers of approximately 10^{-5} and higher. Longest and Xi [105] showed that for the particle with the Stokes numbers smaller than 5×10^{-5}, the effects of particle inertia on area-averaged deposition efficiency could be neglected. Furthermore, Stokes number combined with the evaporation phenomenon affects the possibility of particles with non-volatile nuclei to be airborne if St<<1 [5]. It is worth noting that the Stokes number of particles indicates if a particle falls down or turn to be airborne

Regarding the numerical settings, it should be noted that the most appropriate numerical setting for the CFD simulation of the respiratory events depends on its application, mainly within a short period of time. Hence, an unsteady (transient) framework is suitable since it allows capturing temporal changes in the location and spread (plume shape) of the respiratory event. However, suppose the goal of a study is researching time-averaged or steady-state behavior, such as the effects of ventilation on the spread quality. In that case, steady-state simulations can be employed.

4.2. Turbulence model and near-wall treatment

Turbulence models affect the CFD simulations from two perspectives of accuracy and computational cost (mesh resolution, especially near walls). Hence, to select an appropriate turbulence model, the final application should be taken into account. For example, Bass and Longest [101] showed that the deposition of particles inside upper airways solved by the low Reynolds number (LRN) k-ω model was comparable with the Large Eddy Simulation (LES) while LES was computationally more expensive. In general, in many droplets' transportation and dispersion models, high Reynolds number turbulence models (such as RNG-k-ε and RLZ-k-ε) are appropriate choices. The near-wall mesh resolution can be even larger than $y^+>100$, and the wall function can be employed. However, when accurate results near the solid walls are required, such as particle deposition in airways and lungs, the near-wall mesh resolution must be fine ($y^+ \approx 1$) and low Reynold number turbulence models (such as SST-k-ω) are needed.

In LES, larger eddies can be captured by a generated mesh, whereas the effects of smaller eddies that cannot be resolved are accounted using subgrid scale (SGS) models. Although LES provides the closest results to the Direct Numerical Simulation, it still has some difficulties, especially in predicting correct pressure losses [106]. LES models require very fine meshes near solid walls if the wall functions are not employed. Nevertheless, if wall functions are applied, computational cells can be coarser in the vicinity

of walls, but near-wall properties of a flow cannot be predicted accurately. Finally, for this turbulence model, it is worth mentioning that the effects of the small filtered eddies on the flow field can play a crucial role especially in applications such as near-wall flows [107], reacting flows [108], and multiphase flows [109].

Further to the choice of turbulence models and near-wall treatment, the underlying physics of phenomena related to droplet fluid dynamics should be considered if necessary. These phenomena include droplets' deposition, breakup, collision, and evaporation (for equations, see Appendix II).

It should be mentioned that the effect of the turbulence model on the quality of the dispersion of particles is directly related to the type of the applied turbulence model. For example, LES can solve the background flow field with much smaller and detailed vortices. Hence, the trajectory of particles, especially the local trajectories, will be in more detail. However, since RANS models are based on time-averaged, they provide particles trajectories with fewer details. Hence, if a research task is intended to obtain details of particles trajectories or sedimentations (such as in lungs), LES will provide more details. However, as mentioned above, considering cost and accuracy RANS models are a suitable trade-off for the simulation of droplets by respiratory in indoor and outdoor spaces.

4.3. Deposition and Effects of Air Movement

Droplets released from a patients' mouth can either fall on the ground or stay suspended due to the combination of their weight evaporation and the buoyancy force. Some particles with 30μm<d<100 μm may move downward (due to the gravity), while losing their mass due to evaporation. However, if the buoyancy force becomes dominant before reaching the ground, the falling particle becomes airborne [110].

The deposition also depends on the background air movement and ventilation [101,102,111], and the deposition of particles can increase up to 6.5 m [112] or even 8.1 m [113] from the source. CFD simulations have been used to simulate re-suspension of the deposited particle by setting boundary conditions at the walls, such as bouncing (i.e., [9,112–115]).

4.4 Break-up and Collision of Droplet

The droplet breakup depends upon factors such as velocity, viscosity, pressure difference, and shape of the droplet, which are investigated via Weber number (We) defined as the ratio of disrupting aerodynamics forces to the surface tension forces of the droplet [116]. It has been shown (Appendix II) that droplets have a maximum stable diameter above which their diameter cannot increase without breaking up, and a minimum diameter below which the break-up does not occur. Regardless of this fact, break-up results in the formation of two or more smaller droplets. If the range of particle diameters in a

CFD simulation includes particles with small diameters, it will cover the diameter of the resulting broken particles after a break-up. Hence, the CFD simulation with droplet break-up faces an increase in the computational cost [117–119].

Specifically for respiratory events, a droplet-droplet collision can result in a bigger droplet or a formation followed by a secondary break-up [120–124]. The droplet-droplet collision of respiratory droplets has been investigated by [125–127]. For CFD simulation of a respiratory effect, adding collision increases the computational cost almost pseudo-linearly with respect to the number of particles [128]. Many other documents also confirm the associated cost increase, e.g. [129,130]. If the range of particle diameters in a CFD simulation covers large particles, it can cover the diameter of the resulting particles after the collision.

All in all, in addition to the computational cost, collisions between the respiratory droplets are neglected in many droplets' transport studies due to a low probability of collision because of the low volume fraction of liquids in respiratory jets. As it is shown in Table 2, many CFD studies neglect collision or break-up phenomena in their simulations.

4.5. Evaporation

The respiratory droplet is composed of water, salt, proteins, and pathogens (virus or bacteria) [131] [132]; [133]. The aquatic portion of all particles evaporates during the evaporation, and each droplet shrinks down into a non-volatile nucleus [134]. The changes in the size, mass, and density of the particles change the particles' buoyancy and aerodynamic drag forces and airborne behavior. Since the evaporation of respiratory droplets is the process through which the droplets convert to pathogen-carrying nuclei, solving evaporation equations in a CFD simulation is vital and crucial, as shown in Table 2.

Nonetheless, in a respiratory event, the sizes and volume fraction of droplets are small. Thus, particles' impact on the dynamics of the continuous phase (air) is negligible. As a result, the one-way coupling is a suitable choice for the CFD simulation of air-particle interactions. This option technically means that the interaction between the background flow and particle is such that only the background air affects the particles.

It should be mentioned that many researchers have studied evaporation mainly through numerical simulations. As Vuorinen et al. [5] demonstrated for the evaporation of droplets in stagnant ambient air, droplets with a diameter below 80 μm completely evaporate before they reach the ground surface. In addition, the same research showed that the suspension time varies from above one hour for particles smaller than 10 μm to 2~200 seconds for the particles between 100~200 μm.

Table 2: Consideration of underlying physics in CFD studies of pathogen droplets' transport

Ref.	Particle Size (µm)	Modeling approach	RH (%)	Evap.	Collision	Breakup	Buoyancy	Coupling	CFD approach/ Turb. model
[5]	1-200	Various	0-100	yes	no	no	yes		LES
[6]	3-750	Lagr.*	10 to 90	yes	no	no	yes	one-way	RNG-k-ε
[33]	1-100	Lagr.	35,50,65	yes	no	no	NM§	one-way	LES
[14]	8.3	Lagr.	80-95	yes	no	no	NM§	one-way	RNG-k-ε
[18]	2.5-250	Lagr.	30-60	yes	no	no	yes	one-way	SKE SST-k-ω and RNG-k-ε
[24]	30	Lagr.	no	yes	no	no	yes	one-way	SST-k-ω (low Re)
[40]	1	Lagr.	no	no	no	yes	yes	one-way	RLZ-k-ε
[28]	10	Lagr.	no	no	no	no	yes	one-way	RNG-k-ε
[135]	1-500	Lagr.	20, 40 & 60	yes	no	no	yes	two-way	RNG-k −ε
[136]	10,100	Lagr.	0 and 90	yes	no	no	yes	one-way	RLZ-k-ε
[137]	0.4-10	Lagr.	0-80	yes	no	no	yes	one-way	RNG k-ε
[138]	0-1000	Lagr.	35,65,95	yes	no	yes	yes	two-way	RLZ-k-ε
[113]	0.1-700	Lagr.	20-80	yes	no	no	yes	one-way	RLZ-k-ε

*Lagr.: Lagrangian
§NM.: Not mentioned
SKE: Standard k-ε
LES: Large Eddy Simulation
RNG: Re-Normalisation Group
SST: Shear Stress Transport
RLZ: Realizable

5. Measurement of Pathogen Airborne and Aerosol Droplets

While the present article aims at reviewing CFD modeling of respiratory flows, a brief review of experimental measurement techniques, including their limitations and uncertainties, is conducted as the experimentally measured data are required to set the boundary and initial conditions of CFD models (see Section 6 for details). Moreover, they are used to validate the CFD models, then can be applied to investigate the flow field where measurements cannot be conducted in a new setoff simulation due to the related intensive expenses, practicality, and/or time constraints. Furthermore, some of the clinical data of pathogen transmission, such as the minimum dose of infection, are useful for translating the CFD field data to safety measures such as risk factors. Also, Zoka et al. [113] provided a well-discussed article on risk assessment of bioaerosol transmission from human respiratory events by employing CFD simulation in confined space.

Experimental techniques in this area can either focus on capturing respiratory flows or on characterizing exhaled particles. In the case of droplets, the major concerns are measuring their size distribution,

concentration, and velocity inside the field [139]. Determination of droplets' size distribution and concentration requires the application of invasive methods, while droplets' diameters and velocities are determined by non-invasive methods [140]. On the other hand, the exhaled flow experimental measurement methods concentrate on the flow's field velocity, temperature, and shape [139]. Global flow field techniques are mainly utilized to exploit the shape and propagation of the exhaled flow and its interaction with the background flow of the target environment [140]. Relying on remote observation of the target medium, particle image velocimetry (PIV), particle tracking velocimetry (PTV) and laser Doppler anemometry (LDA), high-speed photography (HSI), and Schlieren photography are among the most widely employed global techniques [140]. However, pointwise measurement techniques focus on acquiring velocity, flow rate, humidity, and temperature at definite discrete points inside the field [140]. Thermocouples and pressure probes are examples of these measurement methods. A review of methods of capturing respiratory airflow and airborne pathogens in different environments is presented in the following sections.

5.1. Measurement of Flow Field

Besides validation of numerical tools, capturing the dynamic behavior of exhaled airflow as a research tool, and studying the interaction of respiratory and background flows are among the objectives of flow field measurement [139]. To achieve more realistic conditions, mannequins or humans are widely used in flow measurement tests at different complexity levels [141].

5.1.1. Test Setups with Mannequins

The generation of realistic droplets size distribution is a challenging task. Thus, tracer gases like SF_6, CO_2, or N_2O are generally used to simulate small droplet nuclei released by mannequins. Pointwise exploiting the flow parameters using anemometers in different field positions is one of the widely used measuring methods in such test setups. However, the typical level of air velocity in enclosed spaces is usually below the range of most sensors. Moreover, those sensors capable of measuring such low-velocity levels can only return the velocity magnitude, which is a source of uncertainty for CFD validations [141]. More advanced methods like PIV, LDA, and HSI can give more precise measurements though at higher costs.

PIV can measure the velocity through dispersing tracer particles into the field excited by laser pulses [142]. As a popular measuring technique, this approach is mainly used to resolve the respiratory field. Feng et al. applied the PIV measurement to capture the exhaled flow of a breathing manikin in isothermal and heated conditions [143]. Marr et al. [144] conducted the PIV measurements in the breathing zone of a thermal mannequin. Wan et al. [61] applied the PIV method to investigate transport

characteristics of droplets and droplets nuclei under different ventilation strategies. Kwon et al. [145] used this measurement technique to analyze the coughing and speaking-induced velocity field near the mouth. Xu et al. [146] applied this method to investigate inhalation and exhalation flow patterns in a realistic human upper airway. One limitation of this method is the size of the exploration window, which may not cover all over the field, and this would not let CFD validation at the far-field. Another critical parameter to consider in using the PIV method is that the obtained images should be recorded with a sufficiently high frequency so that the dynamics of the exhaled jets are mostly captured [147].

LDA is based on the Doppler effect. Similar to the PIV method, it uses tracer particles to measure the flow field velocity. Sun et al. used the LDA method to study indoor transport of droplets expelled by coughing [148]. They measured the maximum initial velocity range and the time duration of coughing activity from several volunteers. One limitation of this method is that it is limited to only measuring one particle's velocity at a time. So, simultaneous capturing of the velocities of different phases is not possible [148].

HSI is used to resolve flow shape, its propagation, including direction and spread angle. This method uses smoke clouds as tracer particles. Gupta et al. [92] applied HSI to specify boundary conditions of human breathing, speaking, and coughing. Bourouiba et al. [149] used a high-speed camera to visualize cough and sneeze at severe expiratory events. Liu et al. [150] utilized HSI to capture the spread and flow structure of cough. For this purpose, they built a cough generator machine. One restriction associated with this technique is that it can only visualize those parts of the field within the smoke clouds [139,147].

5.1.2. Test Setups with Humans

Volunteered humans are used in several test setups to help better understanding of the interaction of exhaled flow with the environment background flow. In these cases, measuring methods based on laser beams are not conducted due to their health and safety issues. So, the advised technique to capture the flow field in these cases is Schlieren imaging. This method is based on thermal differences in the air to refract a light beam resulting in visualization of the airflow [141]. This method has limited accuracy and is suitable for turbulent refractive flows like cough and sneeze [139].

On the other hand, meaningful measurement with this method strongly depends on the temperature difference between exhaled jet and background flow. Therefore, its application is restricted to the initial parts of the exhaled flows where a temperature difference exists. However, this temperature difference vanishes downstream as these two flows are mixed together, and thus, this method cannot be used to measure far-fields. One more point to add is that the uncertainty in the captured velocity profile is

expected since the optical method records a 2D projection of the real 3D flow of the domain [147]. This can be a challenge when this method is applied to validate 3D CFD simulations.

One general challenge in the validation of CFD simulations for exhaled flow fields is related to temperature and humidity fields caused by the interaction of respiratory flow and the environment background flow, which have been barely modeled [140]. Another critical issue in this regard is that the Reynolds number of these flow types is generally low. Therefore, selecting a proper turbulence model to validate the measured field is challenging.

5.2. Measurement of Airborne Pathogens Droplets

As stated earlier, the primary intention of experimental studies on exhaled droplets is to measure their diameters and size distributions. There are also other targets such as understanding the role of pathogen droplets in the propagation of the disease and performance evaluation of different protective methods. These measuring techniques are reviewed below.

5.2.1. Droplet size distribution

Solid and liquid impaction methods are used to measure the exhaled droplets sizes. Implementing a droplet-capturing surface (solid) or liquid bath, they can capture the passing aerosols over them. One limitation of these techniques is that they are incapable of trapping droplets with diameters greater than five microns due to their rapid fall under the effect of gravity. HSI as a more advanced technology has been applied to measure droplets size distribution. However, its accuracy is restricted by the available focal depth. So, it is not able to measure the smaller diameters (i.e., less than 5 microns). Reviewing the related literature shows that a very diverse range of values for droplet size distributions is reported in different studies, which is an important source of uncertainty. Underlying reasons include the limited resolution of different devices, which impose a specific diameter range measurement, health condition and physical properties of the people under the test, evaporation, and condensation of droplets which lowers the accuracy of the test at the initial stages of the respiratory event. This is also the case in measuring the velocity of different exhaled airflow [139].

Besides the velocity level, different people have various timings and consequently different profiles of respiratory events. For instance, different peak times of cough are observed in different people. This will not allow averaging the captured profiles since the resultant profile will be a distorted, unrealistic one. Thus, in this case, a profile near the average behavior is usually selected [151]. Another source of uncertainty in the size distribution of droplets in different exhalation activities is that they are always reported at a certain distance from the mouth or nose exit. The first reason is that the behavior of the droplets at short distances from the release source is deeply affected by the interaction between a person

and its environment background flow. The second reason is that, immediately at the exit, a large irregular and case-dependent volume of fluid encompasses the droplets, which turns into droplets at a short distance from it in which measuring the shape is quite challenging [139]. Hence, these challenges impose a considerable uncertainty in input data for CFD simulations, which can cause significant discrepancies in the validation procedure.

5.2.2. Exhaled droplets dynamics

Respiratory simulators are used to mock exhaled droplet dynamics [151,152]. Due to the absence of human subjects, viral aerosols can also be introduced to these machines to study their life span inside the room with no infection risk. However, simplifications considered in the design of simulators impose some restrictions in the representation of human respiratory activities. In general, these simulators work with a limited range of droplet sizes and cannot generate the whole size range and count of the exhaled particle. Since droplets' airborne behavior mostly relies on smaller droplets, simulators are preferred to cover smaller droplet sizes. On the other hand, respiratory jets have mainly higher temperature levels compared with the environment. At the same time, simulators barely consider this temperature difference, and therefore the impact of buoyancy is not well represented. Another issue is that the complex and time-dependent behavior of human nose and mouth, which have an important impact on exhaled droplets properties that built simulators cannot replicate even with imposing the same exhalation areas. Besides the existing uncertainty in respiratory time-velocity profiles as discussed in the previous section, the droplets release rate is not uniformly distributed within the exhalation activity timespan [147,151]. In the case of cough, most particles are emitted at the initial stage of a cough. So, this increases the complexity and costs of respiratory simulators [153].

Aside from the available methods to measure the velocity and size of the exhaled droplets inside the flow field in simulators, as explained earlier, one can name particle tracking velocimetry (PTV) and phase doppler anemometry (PDA). PTV does not require particles to be uniformly distributed in the field. Thus, tracking the particles' velocity vector inside the domain enables the validation of Lagrangian models [154]. Janke et al. [155] applied an in-house developed PTV algorithm to capture oscillating flow inside the human mouth. Bahl et al. [156] applied the PTV method to investigate the motions of sneeze droplets. They showed that less than 1% of droplets have velocities larger than 10 m/s while around 80% of droplets travel at velocities less than 5 m/s. Elcner et al. [142] applied the PDA method to validate their CFD model of human tracheobronchial airways. They used a complete inspiration/expiration breathing cycle and included both sedentary and deep breath modes.

As seen earlier, test conduction in simulators is repeatable, and uncertainties seem to be considerably less than what is observed in the case of human subjects. Nevertheless, there are still challenges to validate CFD models with controlled test conditions inside the simulators. First, most particles inside the simulator test chamber have an ultimate diameter of less than 0.1 micrometer [151]. Another source of uncertainty is related to the non-evaporated fraction of respiratory droplets, which is the size of airborne nuclei. The next important limitation is associated with the fact that the discrete phase Lagrangian method should be applied with caution as the droplets streamlines are highly sensitive to the selected parameters in the CFD model.

6. Clinical Inputs of CFD Models and related uncertainties

CFD simulations are highly sensitive to input data used as the model's boundary conditions and material properties. As the released droplet jet from a bio-source, these input data depend on demographical factors such as age, gender, infection condition, and environmental parameters such as ambient temperature, relative humidity, etc., as summarized in Table 3.

Table 3: List of effective factors on the released droplet jet from a bio-source.

#	Item [unit]	Interval	Reference
1	Droplet size distribution [μm]	0.5 – 2000 + (Table 8, Table 9)	[135],[151] + [157]
2	Number of droplets/particles	5000, 9×10^6	[135], [158]
3	Indoor/outdoor space	Different Boundary Condition.	[159]
4	Local ambient air velocity[m/s]	[0.25-1.5], 21.7, 0- 10	[33], [158]
5	Local ambient air direction [deg]	0 -180	[160]
6	Local ambient air humidity [%]	[20 – 60], 50	[135], [33]
7	Local air temperature [^{o}C]	[17-23], 25,	[33], [158]
8	Temporal profile of exhalation [Lit/min]	Fig.2, Fig. 3(a-c)	[161], [33], [162]
9	Spatial profile of exhalation [-]	Fig. 9	[145], [163]
10	With or without facial-mask	[with or without]	[162], [159]
11	Gender [-]	Man, Woman	[161], [145]
12	Age [year]	10 – 70	[164]

Falsified or simplified data can dominantly impact the outcome of a CFD simulation even though all the steps in the pre-processing, processing and post-processing are carefully performed [165,166]. Clinical information and flow field data, as the boundary conditions to be set in the mouth or skin of airborne pathogen bio-sources, have been widely investigated in the past decades [163,167,168]. Nonetheless, when it comes to smaller droplets and aerosols, the rendered measurement techniques, as described in the preceding section, face several technical challenges to ensure the robust presentation of deemed

information. This partially justifies the contradictory data seen in numerous related studies [157]. Moreover, bio-sources are uncontrollable complex organic systems that produce diverse droplet release modes in laboratory experiments even under similar circumstances. Hence, statistical analysis is implemented to translate disparate collected observational data to mathematical functions suitable for being used in the CFD models as (1) temporal velocity profile and, (2) distribution of droplet size, (3) velocity angle, and (4) flow rate and initial velocity. All of these parameters are investigated under different respiratory modes of inhalation, exhalation, speaking, cough, and sneeze. This section, thus, summarizes some of these studies.

6.1. Temporal Velocity Profile

On average, a normal cough has a fraction of the maximum volume of human exhalation, while a normal sneeze is approximately equal to its whole maximum volume. These volumes for men and women are 4.70 L and 3.63 L, respectively [135]. The transient semi-sinusoidal profile airflow rate is the primary and essential feature of cough and sneeze [161]. The most important characteristics of the exhalation profile are expired volume (EV), peak flow rate (PFR), and peak velocity-time (PVT). Several experimental and/or numerical studies have provided empirical values or correlations for PVT, cough PFR (CPFR), and cough EV (CEV) based on the demographic distribution of bio-sources [33,161,162].

An experimental cough aerosol detection via laser diffraction system from 45 healthy people presented a demographic statistical analysis of the droplet size correlated to participants′ gender and age [164]. Busco et al. [138] did experimental and theoretical research for realistic modeling of a human sneeze. They employed a micro-dynamic pressure transducer in order to measure the dynamic pressure of human sneezing. The fitting curve of this study is illustrated in Fig. 2, and it can be formulated as:

$$P(t) = \frac{c_1 t^{a_1-1} e^{\frac{-t}{b_1}}}{b_1^{a_1} \Gamma(a_1)} + \frac{c_2 t^{a_2-1} e^{\frac{-t}{b_2}}}{b_2^{a_2} \Gamma(a_2)} \tag{18}$$

where Γ is the gamma function. $a_1=4$, $b_1=0.0235$ s, $c_1=860.107$ Pa.s, $a_2=9$, $b_2=0.028$ s, and $c_2= 674.3917$ Pa.s. The R^2 value of the fitting curve was 0.9937 with the standard deviation of 0.34 kPa.

Distribution of droplet aerosols in an air-conditioned room by Large Eddy Simulation (LES) CFD model coupled with the Lagrangian method was conducted and validated through experiments by Zhang et al. [33]. They used the profile of Fig. 3 to calculate the temporal cough velocity.
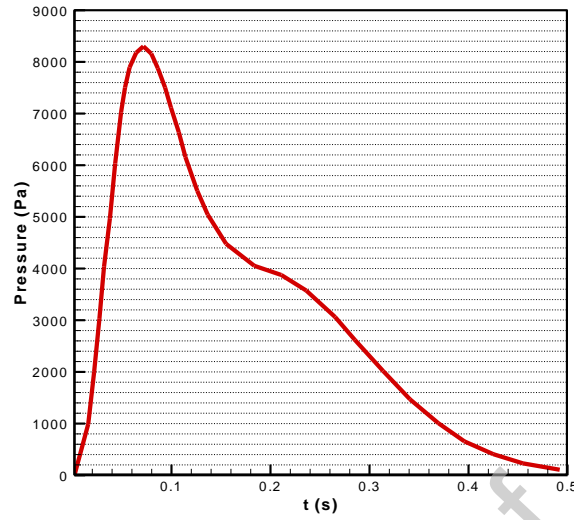
Fig. 2: Fitting curve to the experimental data for the dynamic pressure distribution of human sneeze [138].
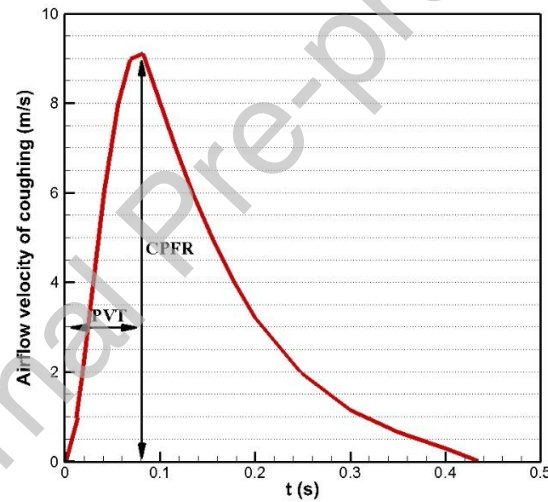

Fig. 3: Temporal velocity profile of cough extracted from [33].

Another experimental research measured the airflow rate of cough while the CPFR value was found to be equal to 8.2 Lit/s, as presented in Fig. 4 (a). In this figure, although the presented total cough duration is higher than 0.5 s, considering that the flow rate of less than 50 L/min falls within normal breathing, the main cough event falls within 0.5 s. In another study, Ren et al. [161] numerically simulated the cough clearance process to quantify the cough effectiveness, as shown in Fig. 4(b). The exhalation part can be simplified and modeled by a linear function as follows:

$$Q = \begin{cases} \dfrac{CPFR}{PVT}(t - t_o) & if\ (t - t_o) \leq PVT \\ \dfrac{-CPFR}{T - PVT}(t - t_o - PVT) + CPFR & if\ (t - t_o) > PVT \end{cases} \tag{19}$$

where t_o is the start of the cough and can be simply assumed to be zero (t_o=0, start of the measurement). The total temporal duration of the cough is considered as t_{tot}=0.5 s [from 0.63s to 1.13s].

Moreover, the initial velocity of jet droplets exhausting from the mouth could be obtained by dividing the flow rate value from Eq. (19) by the cross-section area of the semi-open mouth or trachea. The amount of PVT for males and females is also provided by Gupta et al. [92] as a function of CPFR through curve fitting from extensive experimental data (see Fig. 4(c)):

$$PVT = 3.152 \times CPFR + 64.63 \ (female)$$
$$PVT = 1.360 \times CPFR + 65.86 \ (male)$$

(20)

where the PVT and CPFR values are in *ms* and *L/s* units, respectively.

Zhang et al. [33] numerically simulated breathing with the profile of Fig. 5(a) as the human periodic breathing cycle. Villafruela et al. [163] conducted an experimental study for the breathing mode of exhalation only by neglecting the inhalation period. They replicated the human breathing via their experimental manikin setup in which breathing was reported in a shape of a sinusoidal function with respect to time. Their results can be fitted to the shape of the temporal breathing velocity amplitude [163] (see Fig. 5(b)):

$$V_{mouth} = \begin{cases} 0 & if \ v < 0 \\ 4.5.\sin(1.79t) & if \ v > 0 \end{cases}$$

(21)

where *t* is the time (s).

Berlanga et al. [169] performed a numerical-experimental investigation on the hydrodynamics of exhalations. They used a manikin and utilized PIV to identify the transient puff structures for two different modes of activities, including standing, relaxed, and walking. They presented the exhalation profile as demonstrated in Fig. 5(c), in which the mouth area was set to 260 mm^2. Furthermore, the breathing velocity of 1.3 m/s with a maximum propagation distance of 0.8 m is reported by [170], in which the authors extracted sneezing data from six people (2 women and 4 men) who attended their experiments.
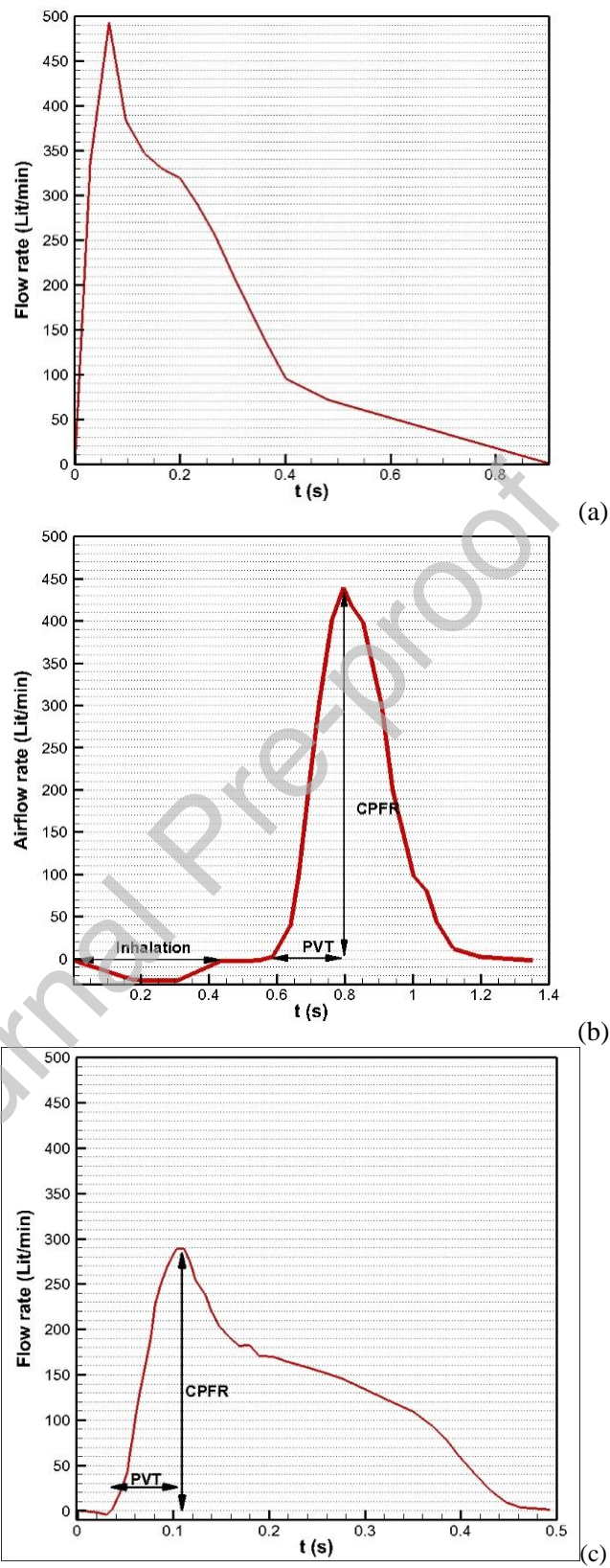
(a)

(b)

(c)

Fig. 4: Distribution of temporal cough airflow rate extracted from (a) [162], (b) [161], and (c) [92].
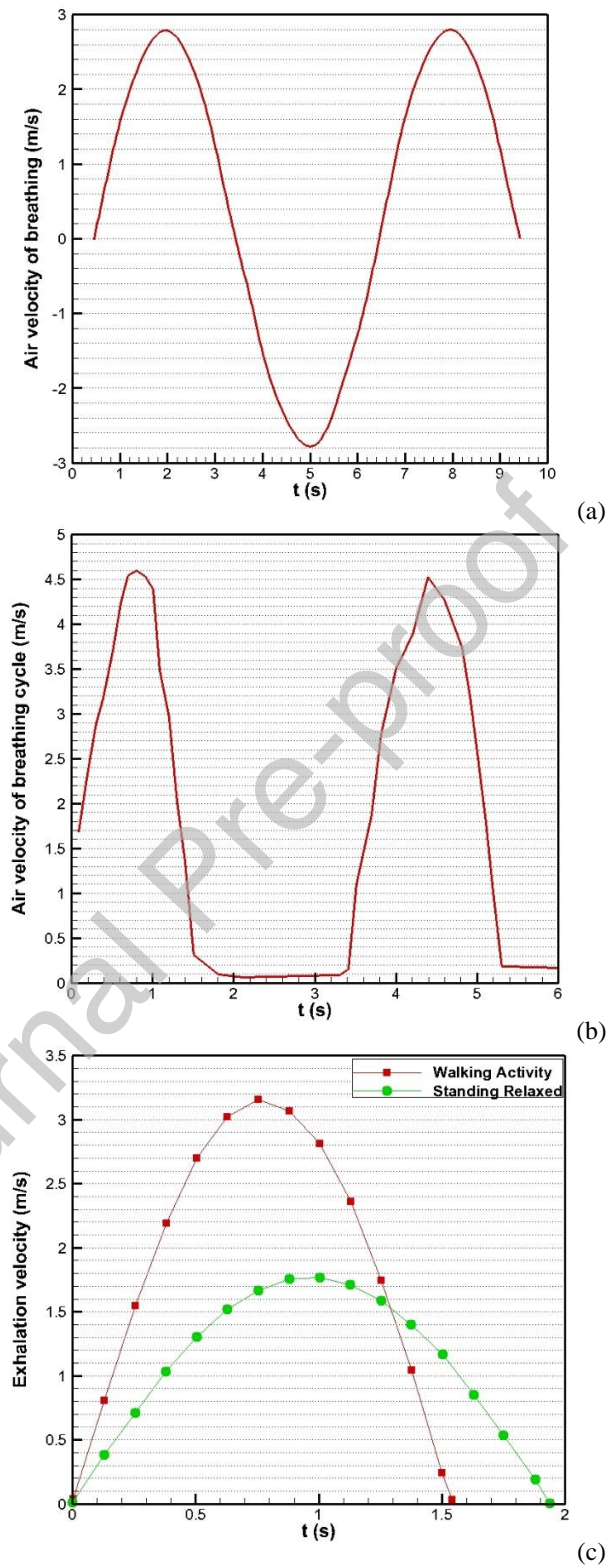
(a)

(b)

(c)

Fig. 5: Temporal velocity distribution of breathing cycle extracted from (a) [33], (b) [163], and (c) [169]

Xie et al. [161] estimated the velocity of large particles dispersed during sneezing to be about 50 m/s. Based on the experimental results of Jennison and Edgerton [171] for sneezing, the exhaled droplet speed could reach up to 46 m/s. The airflow rates at a mouth cross-section for the case of sneezing were experimentally measured by Mortazavy et al. [172]. They measured the outlet flow rate with a Spirometer device while the mean maximum and average flow rates were obtained as 10.58 L/s and 4.79 L/s, respectively. The summary of the maximum sneeze velocity or airflow rate at a mouth is given in Table 4.

Table 4: Summary of the maximum sneeze velocity at a mouth.

Item	1	2	3[+]	4	5	6[+]
Velocity or Flowrate	50[m/s]	46[m/s]	10.58 [L/s] 4.79 [L/s]	48.3 [m/s]	35.5 [m/s]	23.5 [L/s] 18.15 [L/s]
Ref.	[131]	[171]	[172]	[86]	[149]	[135]

[+]By assuming a realistic mouth area (e.g., 260 mm^2[169] or 128 mm^2[138]), one may compute inlet velocity.

Nonetheless, other values have been reported for the velocity of respiratory events in the literature, but due to their significant differences, they have been treated as outliers in Table 5. Moreover, the velocity of the breathing mode is reported in the literature and presented in Table 6. As it can be seen, there is a relatively wide range of velocity reported from 1.8 m/s to 4.5 m/s.

Table 5: The other value reported for sneeze velocity.

Sneeze velocity at mouth [m/s]	Mouth area [cm^2]	Year – [Ref.]
5.3, 11.5 (corresponding to min & max value reported in [172])	9.22	2019 – [173]
4.5	-	2013 – [170]
100	-	1955 – [174]

Table 6: Summary of the maximum breathing velocity at a mouth.

Item	1	2	3
Velocity (m/s)	1.8	2.8	4.5
Ref.	[169]	[33]	[163]

Finally, Table 7 presents the most frequent values reported in the literature for four different exhalation modes, including breathing, speaking, coughing, and sneezing. The given ranges may depend on many demographic factors, such as gender and age and posture and health condition.

Table 7: Most reliable velocity interval for each mode of exhalation synthesized from [33,86,163,169,171,172,92,131,135,138,145,149,161,162]

	Breathing	Speaking	Coughing	Sneezing
Velocity range (m/s)	0 -2.8	2.5-4	8-14	18-50

The reported data for the velocity angle of the airborne pathogen droplets are limited in the literature. In an experimental study by Kwon et al. [145] using PIV and climate chamber with a constant temperature of 23 ^{o}C and relative humidity of 50%, the average initial velocity for coughing mode of exhalation was measured as 10.6 m/s and 15.3 m/s for females and males, respectively. The measurement area was 247 mm × 184 mm located in front of the mouth opening. In addition, the average initial velocity for the speaking mode of the exhalation for females and males was reported as 2.31 m/s and 4.07 m/s, respectively. The exhaled air angle from coughing was observed to be around 38 ^{o} for the males and 32 ^{o} for the females, while that of the exhaled air from the speaking mode was around 49° and 78°, respectively (see Fig. 6). As reported, 26 people, consisting of 17 males and 9 nine females, participated in performing the experiments three times in the front side of the chamber.

	Male	Female
θ_{up}	19.9	15.0
θ_{down}	17.9	17.3
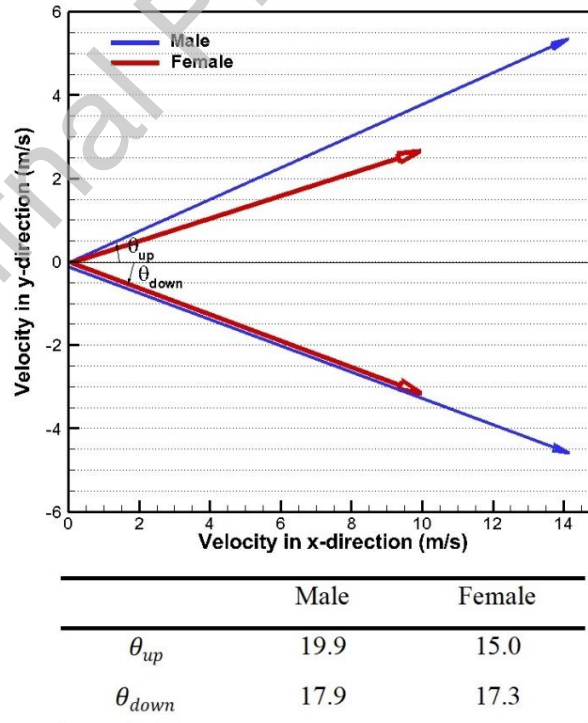
Fig. 6: Initial coughing velocity extracted from [145].

6.2. Distribution of Droplet Size

A review of the literature before 2015 on respiratory droplet characteristics highlights that the droplet size of breathing may vary between 0.3 to 5 µm while there is a noticeable uncertainty on the size of the largest droplets as they were reported around 10 µm [175]. In another study, a human-like aerosol cough simulator placed in a controlled environment was employed to record the droplet size distribution of cough caused by influenza patients [151]. The total aerosol volume collected in each cough was equal to 68 µL. Also, in their experiment, the cell culture medium[1] was employed as a surrogate for liquid aerosol production. The airflow rate of the airbrush was approximately found to be 8.4 L/min at 138,000 Pa (operating pressure). Another experiment was conducted for the droplet size distribution measurement of the sneeze mode right at mouth opening by recruiting twenty healthy people, consisting of 10 males and 10 females in the ages of 16–25 [8]. With no history or evidence of significant pulmonary diseases, these participants released 44 sneezes measured by a laser particle size analyzer. Two types of distributions were observed, including unimodal and bimodal, as shown in Fig. 7. The unimodal distribution was found as:

$$P_i = \left(\frac{A_u}{\sqrt{2\pi}\sigma_u}\right) e^{-(Log(D_i)-\mu_u)^2/2\sigma_u^2} \tag{22}$$

where P_i [%] is the volume ratio of all the particles within the category of diameters in size class i to the total volume of all the particles. D_i [µm] is the averaged diameter of a size class i. It is also reported that the mean is μ_u=2.7264, and the variance is $\sigma_u = 0.1523$ [8].

<div style="border-top:1px solid #000; width:30%;"></div>
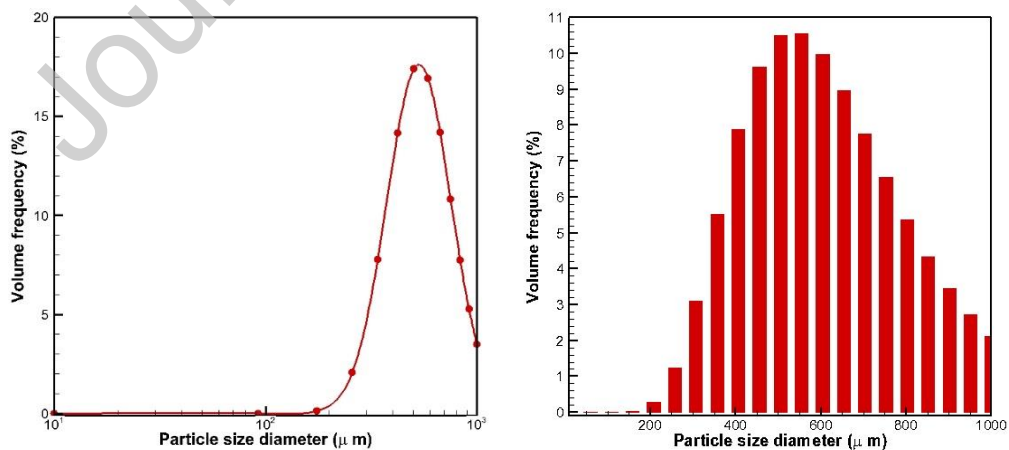
[1]Complete Dulbecco's Modified Eagle Medium (CDMEM) consisting of Dulbecco's Modified Eagle Medium, 100 U/ml penicillin G, 100 µg/ml streptomycin, 2 mM L-glutamine, 0.2% bovine serum albumin, and 25 mM HEPES buffer.

Fig. 7: Reproduction of particle size distribution from Eq. (22).

For the unimodal distribution, the sum of the volume frequency in all the size classes is 1 (100%), so the coefficient of the unimodal distribution can be calculated according to the mean and variance as expressed by [8]:

$$A_u = 100\sqrt{2\pi}\sigma_u \left(\sum_{i=1}^{n} e^{-(Log(D_i)-\mu_u)^2/2\sigma_u^2} \right) \qquad (23)$$

Chao et al. [157] rearranged the particle size distribution of the sneeze mode from Busco et al. [138] and classified them into the 15 bins, from class 3 µm to class 750 µm, as shown in Table 8.

Table 8: Particle distribution measured for sneezing [157].

Size range [µm]	Size class / mean	Frequency of Sneezing
2 – 4	3	0
4 – 8	6	7706.95
8 – 16	12	23491.91
16 – 24	20	26203.62
24 – 32	28	25689.82
32 – 40	36	24933.4
40 – 50	45	24176.97
50 – 75	62.5	58344.43
75 – 100	87.5	33054.23
100 – 125	112.5	41703.14
125 – 150	137.5	32540.44
150 – 200	175	41588.96
200 – 250	225	44129.41
250 – 500	375	179257.9
500 – 1000	750	193444.3
	Sum	756265.5
	Mean	50417.69833

Moreover, Chao et al. [157] provided distribution for the particle size emitted from a mouth during cough and speaking modes of exhalation as presented in Table 9.

Table 9: Concentration of particle count extracted from [157]

Size range	Size class / mean	DNC of Speaking	DNC of Coughing
2 – 4	3	4.59	86
4 – 8	6	66.21	1187
8 – 16	12	22.23	444
16 – 24	20	11.33	144
24 – 32	28	7.87	54
32 – 40	36	4.32	50
40 – 50	45	4.47	41
50 – 75	62.5	4.57	43

75 – 100	87.5	3.44	30
100 – 125	112.5	4.52	36
125 – 150	137.5	4.31	34
150 – 200	175	4.52	93
200 – 250	225	3.85	53
250 – 500	375	3.45	44
500 – 1000	750	1.11	30
	Sum	150.8	2368
	Mean	10.05266667	157.9333333
	SD	15.773871	292.8805141

DNC = Droplet Number Concentration

In a recent numerical investigation, Dbouk and Drikakis [176] applied a total number of 1,008 exhaled droplets equal to 7.7 mg per cough and used the Weibull distribution for the probability density function (see Eq. (24)) for distribution of the initial droplet size. Furthermore, the mouth opening was considered a rectangle with a length of 4 cm and a length to height ratio of 8.26. Also, a transient velocity with a maximum velocity of 8.5 m/s was set at the mouth outlet:

$$f = \frac{n}{\bar{\bar{d}}_p}\left(\frac{d_p}{\bar{\bar{d}}_p}\right)^{n-1} e^{-\left(\frac{d_p}{\bar{\bar{d}}_p}\right)^n}, \quad n = 8, \bar{\bar{d}} = 80 \ \mu m \tag{24}$$

In another study, Lindsley et al. [7] carried out an experimental study over several participants on the particle size distribution using a laser aerosol particle spectrometer with a size range of 0.35 to 10 μm. They collected the data for two conditions of being infected by Influenza and after being recovered, as illustrated in Fig. 8. A meaningful difference between these two conditions was reported such that the ill people produced a significantly greater volume of aerosol. Another important fact reflected from this research is the considerable uncertainty in the reported number of particles at each size bin, irrespective of underlain conditions. As an example, in the bin of (0.35-0.37 μm), the number of particles varies from approximately 3,900 to 10,200. Moreover, by comparison of the reported data in [7] and [138], one may notice another important difference, which is the existence of submicron bins in [7]. It must be mentioned that, as all particles in the experiments of [7] undergo the evaporation process, most of the submicron particles were not submicron at the mouth outlet. This point is crucial, especially for setting the boundary condition at the mouth outlet in the CFD models. By examining the experimental setup of [7], one may see that the employed particle spectrometer is connected to a chamber while the flow of cough passes through an ultrasonic spirometer as it enters the collection chamber for the cough aerosols analysis. In other words, considering the rapid evaporation of micron-size droplets, particle size distribution at the mouth opening is completely different from the presented distribution.

The data variation and uncertainty are not only limited to the distribution of particles. The total number of expelled droplets varies from one person to another, as seen in Fig. 9. In this experimental study, nine volunteers (subjects) were selected and asked to cough during influenza and after recovery. While subject No.5 expels an average of 300,000 droplets, the number of expelled droplets by No. 1, 4, and 9 is almost negligible. The average of 75,400 particles per cough from 0.35 to 10 μm in optical diameter with a standard deviation of 97,300 is reported, which shows a considerable diversity and uncertainty although their instrumentation has good precision. In fact, this uncertainty is more connected to the nature of this phenomenon than measuring instrumentation, which makes the experiment's repeatability difficult. This area is featured by the inherent uncertainty associated with the demographical properties of respiratory events such as sneeze and cough.
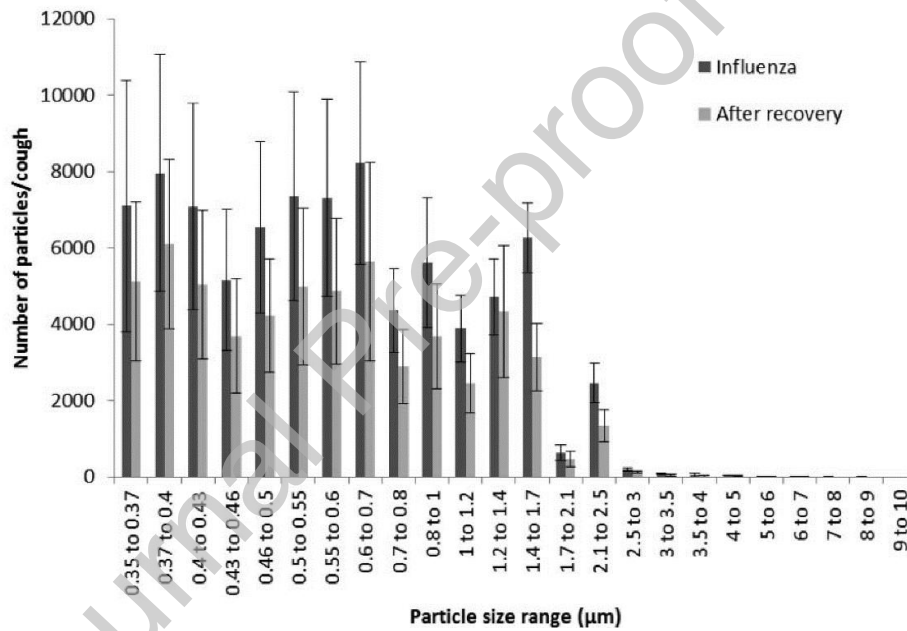
Fig. 8: Distribution of particle size for two conditions of participants being infected by Influenza and after their recovery [7].
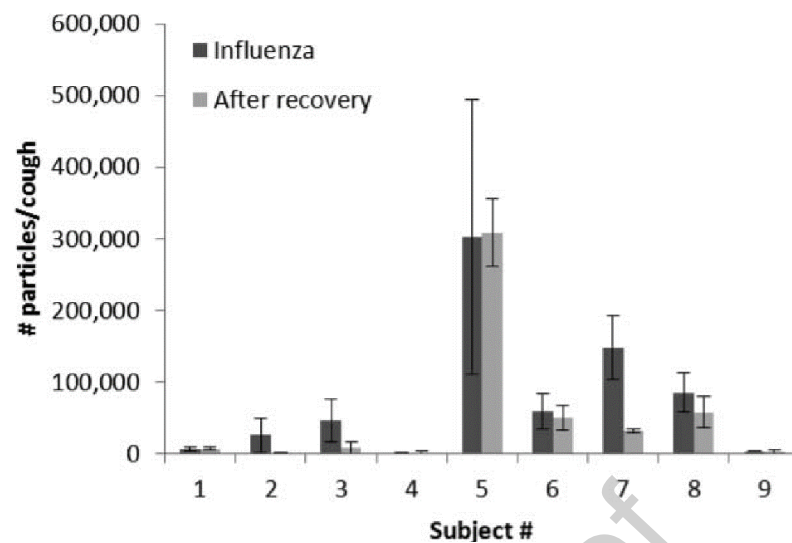
Fig. 9: Total number of particles per cough expelled within the range of 0.35 to 10 μm [7].

The collection of droplets in the exhaled air has been considered as a new method for sampling respiratory particles [177]. Using this technique, particle mass per liter for a breathing mode was measured with respect to the maximum expiratory flow [178]. Nonetheless, this study has shown no significant correlation (Pearson Co. = 0.221) between particle concentration and the maximum exhalation flow rate using linear regression as reported in Fig. 9 (see red line). This experimental report hence admits the broad innate uncertainties in collecting the clinical data related to exhalation modes, as seen in Fig. 10.
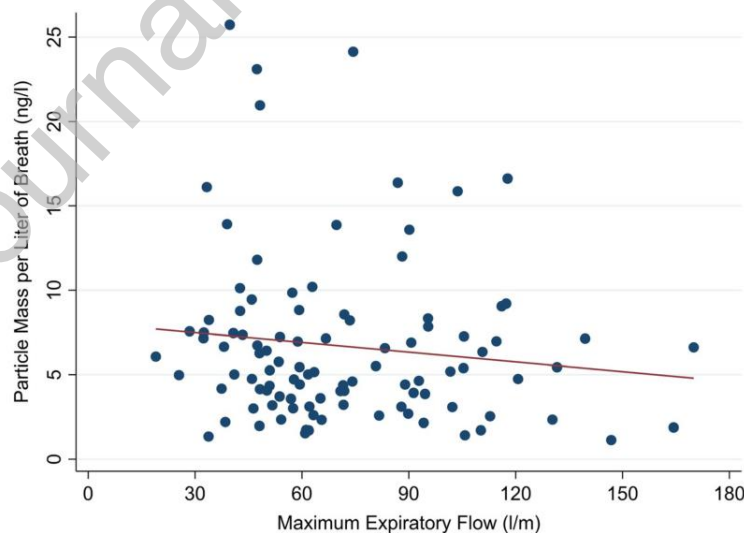
Fig. 10: The exhaled particles mass for the breathing mode of exhalation in relation to the maximum exhalation flow rate [178].

In a recent investigation, Alsved et al. [179] performed an experimental investigation on exhaled respiratory droplets by recruiting 12 volunteers, including seven opera singers and five non-professional

ones sitting or standing upright in a conditioned room 22 ^{o}C and RH=40%. They employed an aerodynamic particle sizer (APS, Model 3321, TSI Inc.) to measure the particle size and concentration in the interval of 0.5–10 µm within a five-second span. As seen in Fig. 11, their results show a few small particle sizes for breathing. As the intensity of the vocal cord activity increases, the number of emitted particles as well as their mass rates are observed to be increased [179]. In another study, Wan et al. [180] reported breathing particles' size and concentration distribution for a patient in a room under two different modes of mechanical ventilation, including pressure and volume control. As seen in Fig. 12, the particle size distribution profiles for both ventilation modes resemble such that the detected difference can only be found in the small-size particles (0.2-0.3 µm) [180].

(a)   (b)
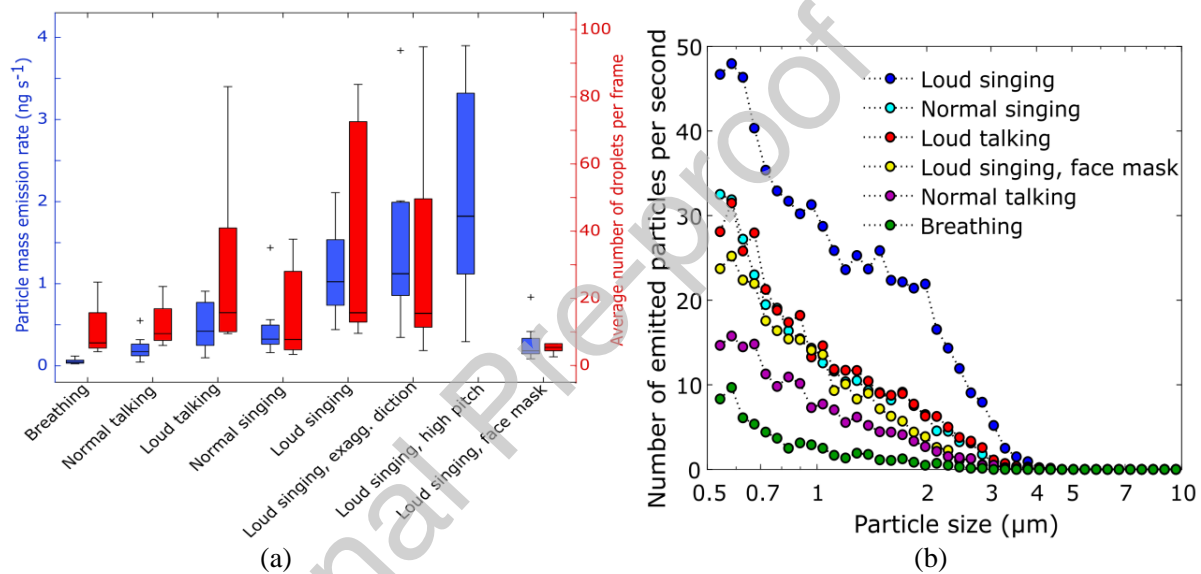
Fig. 11: (a): The particle mass emission rates for different modes of exhalation, and (b): Median number of emitted particles in size range 0.54–10 µm per second for the 12 singers [179].
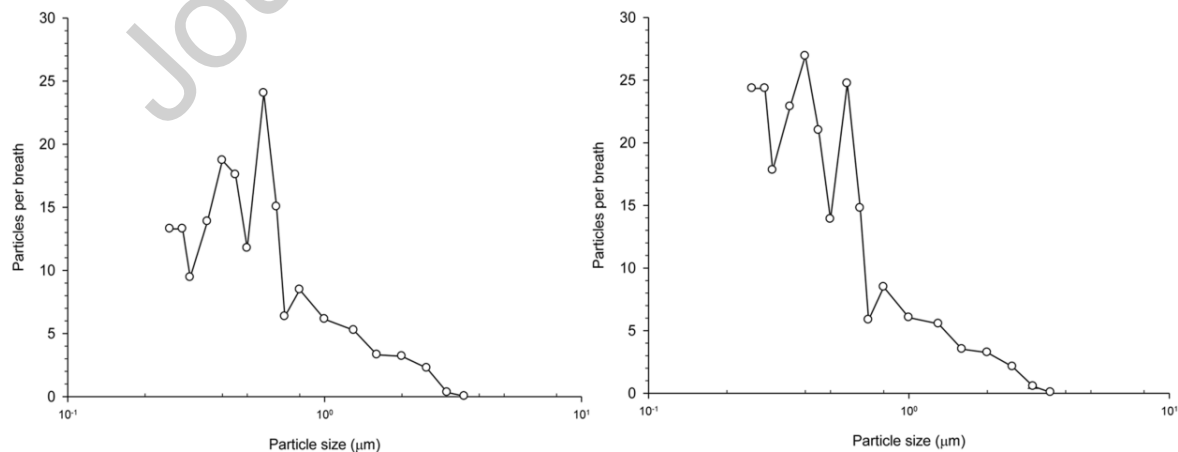
Fig. 12: Size concentration distributions of a patient in a mechanically ventilated room with (a) pressure control mode and (b) volume control mode [180].

7. Conclusion and Remarks

CFD has been recognized as an inexpensive tool to accurately simulate various airborne pathogen transmission scenarios. Nonetheless, accurate CFD modeling demands feeding reliable input data to the developed models. Hence, this paper has initially reviewed the relevant studies related to the transmission of airborne and aerosols originating from respiratory events to extract details of essential clinical parameters needed as inputs to the CFD models. It further has investigated the inherent limitations associated with the CFD modeling and the associated experimental studies, including oversimplification of the underlying physics and the inherent uncertainty in the experimentally measured data.

The first limitation is connected to the high complexity of the interdisciplinary nature of the aerosol transition. This multi-physics problem includes transient 3D multiphase turbulent flow, undergoing the evaporation process within a relatively large volume of the case studies while very small simulation time-steps are needed.

According to the literature, although a specific interval for the velocity variation is presented for each respiratory event, the reported values are still far beyond being in reliable intervals. In fact, the uncertainty of the clinical data is more connected to the nature of respiratory phenomena rather than measuring instrumentation. Respiratory events such as sneeze and cough are characterized by the inherent uncertainty associated with the demographical characteristics such as gender, age, and health condition of a person. Therefore, to draw an inclusive conclusion, e.g., to issue a new protocol, a wide range of data must be taken into account, and depending on the severity of the situation, considering whether vulnerable people are involved or not, modeling could be based on the worst-case scenario or based on averaged-value scenario to make it more economical.

References

[1]   J.J. Klemeš, Y. Van Fan, R.R. Tan, P. Jiang, Minimising the present and future plastic waste, energy and environmental footprints related to COVID-19, Renew. Sustain. Energy Rev. 127 (2020). https://doi.org/10.1016/j.rser.2020.109883.

[2]   C. Zhou, G. Yang, S. Ma, Y. Liu, Z. Zhao, The impact of the COVID-19 pandemic on waste-to-energy and waste-to-material industry in China, Renew. Sustain. Energy Rev. 139 (2021) 110693. https://doi.org/10.1016/j.rser.2020.110693.

[3]   C. Zanocco, J. Flora, R. Rajagopal, H. Boudet, Exploring the effects of California's COVID-19 shelter-in-place order on household energy practices and intention to adopt smart home technologies, Renew. Sustain. Energy Rev. (2020) 110578. https://doi.org/10.1016/j.rser.2020.110578.

[4]   WHO, Modes of transmission of virus causing COVID-19: implications for IPC precaution recommendations, WHO. (2020). https://www.who.int/news-room/commentaries/detail/modes-of-transmission-of-virus-causing-covid-19-implications-for-ipc-precaution-recommendations.

[5]   V. Vuorinen, M. Aarnio, M. Alava, V. Alopaeus, N. Atanasova, M. Auvinen, N. Balasubramanian, H. Bordbar, P. Erästö, R. Grande, N. Hayward, A. Hellsten, S. Hostikka, J. Hokkanen, O. Kaario, A. Karvinen, I. Kivistö, M. Korhonen, R. Kosonen, J. Kuusela, S. Lestinen, E. Laurila, H.J. Nieminen, P. Peltonen, J. Pokki, A. Puisto, P. Råback, H. Salmenjoki, T. Sironen, M. Österberg, Modelling aerosol transport and virus exposure with numerical simulations in relation to SARS-CoV-2 transmission by inhalation indoors, Saf. Sci. 130 (2020) 104866. https://doi.org/10.1016/j.ssci.2020.104866.

[6]   Y. Yan, X. Li, J. Tu, Thermal effect of human body on cough droplets evaporation and dispersion in an enclosed space, Build. Environ. 148 (2019) 96–106. https://doi.org/10.1016/j.buildenv.2018.10.039.

[7]   W.G. Lindsley, T.A. Pearce, J.B. Hudnall, K.A. Davis, S.M. Davis, M.A. Fisher, R. Khakoo, J.E. Palmer, K.E. Clark, I. Celik, C.C. Coffey, F.M. Blachere, D.H. Beezhold, Quantity and size distribution of cough-generated aerosol particles produced by influenza patients during and after illness, J. Occup. Environ. Hyg. 9 (2012) 443–449. https://doi.org/10.1080/15459624.2012.684582.

[8]   Z.Y. Han, W.G. Weng, Q.Y. Huang, Characterizations of particle size distribution of the droplets exhaled by sneeze, J. R. Soc. Interface. 10 (2013). https://doi.org/10.1098/rsif.2013.0560.

[9]   STAR-CCM, STAR-CCM+ Ver. 13.06.012 user guide, n.d.

[10]   Scientific Brief: SARS-CoV-2 and Potential Airborne Transmission, (n.d.).

[11]   L. Morawska, Droplet fate in indoor environments, or can we prevent the spread of infection?, in: Proc. Indoor Air 2005 10th Int. Conf. Indoor Air Qual. Clim., 2005: pp. 9–23.

[12]   W. McKibbin, R. Fernando, The economic impact of COVID-19, Econ. Time COVID-19. 45 (2020).

[13]   M.A. Kohanski, L.J. Lo, M.S. Waring, Review of indoor aerosol generation, transport, and control in the context of COVID- 19, Int. Forum Allergy Rhinol. 10 (2020) 1173–1179.

https://doi.org/10.1002/alr.22661.

[14] H.C. Yu, K.W. Mui, L.T. Wong, H.S. Chu, Ventilation of general hospital wards for mitigating infection risks of three kinds of viruses including Middle East respiratory syndrome coronavirus, Indoor Built Environ. 26 (2017) 514–527.

[15] H. Qian, X. Zheng, Ventilation control for airborne transmission of human exhaled bio-aerosols in buildings, J. Thorac. Dis. 10 (2018) S2295.

[16] T.N. Verma, A.K. Sahu, S.L. Sinha, Study of Particle Dispersion on One Bed Hospital using Computational Fluid Dynamics, in: Mater. Today Proc., Elsevier Ltd, 2017: pp. 10074–10079. https://doi.org/10.1016/j.matpr.2017.06.323.

[17] R. Yam, P.L. Yuen, R. Yung, T. Choy, Rethinking hospital general ward ventilation design using computational fluid dynamics, J. Hosp. Infect. 77 (2011) 31–36. https://doi.org/10.1016/j.jhin.2010.08.010.

[18] L. Anghel, C.-G. Popovici, C. St\uatescu, R. Sasc\uau, M. Verdeş, V. Ciocan, I.-L. Şerban, M.A. M\uar\uanduc\ua, S.-V. Hudişteanu, F.-E. Ţurcanu, Impact of HVAC-Systems on the Dispersion of Infectious Aerosols in a Cardiac Intensive Care Unit, Int. J. Environ. Res. Public Health. 17 (2020) 6582.

[19] A.K. Sahu, T.N. Verma, S.L. Sinha, Numerical Simulation of Air Flow in Multiple Beds Intensive Care Unit of Hospital, Int. J. Automot. Mech. Eng. 16 (2019) 6796–6807.

[20] M.K.H. Leung, O.K.Y. Chau, L.C. Ho, Local exhaust ventilation for infection control in hospitals, HKIE Trans. 12 (2005) 27–32.

[21] T.T. Chow, Z. Lin, W. Bai, A. Kwan, Design and performance of a negative pressure operating theatre, HB 2006-Healthy Build. Creat. a Heal. Indoor Environ. People, Proc. 4 (2006).

[22] J.-I. Bang, J. Park, A. Choi, J.-W. Jeong, J.Y. Kim, M. Sung, Evaluation of UR-UVGI system for sterilization effect on microorganism contamination in negative pressure isolation ward, Sustainability. 10 (2018) 3192.

[23] S. Zhu, J. Srebric, J.D. Spengler, P. Demokritou, An advanced numerical model for the assessment of airborne transmission of influenza in bus microenvironments, Build. Environ. 47 (2012) 67–75. https://doi.org/10.1016/j.buildenv.2011.05.003.

[24] L. Zhang, Y. Li, Dispersion of coughed droplets in a fully-occupied high-speed rail cabin, Build. Environ. 47 (2012) 58–66. https://doi.org/10.1016/j.buildenv.2011.03.015.

[25] Z. Han, G.N.S. To, S.C. Fu, C.Y.-H. Chao, W. Weng, Q. Huang, Effect of human movement on airborne disease transmission in an airplane cabin: study using numerical modeling and quantitative risk analysis, BMC Infect. Dis. 14 (2014) 1–19.

[26] A.M. Farag, E.E. Khalil, Numerical analysis and optimization of different ventilation systems for commercial aircraft cabins, in: 2015 IEEE Aerosp. Conf., 2015: pp. 1–12.

[27] K.K. Coleman, W. V Sigler, Airborne influenza A virus exposure in an elementary school, Sci. Rep. 10 (2020) 1–7.

[28] G.H. Feng, Y. Zhang, X.Y. Lan, Numerical study of the respiratory aerosols transportation in ventilated classroom, in: Appl. Mech. Mater., 2012: pp. 4298–4304.

[29] Q. He, J. Niu, N. Gao, T. Zhu, J. Wu, CFD study of exhaled droplet transmission between occupants under different ventilation strategies in a typical office room, Build. Environ. 46

(2011) 397–408. https://doi.org/10.1016/j.buildenv.2010.08.003.

[30] P. Azimi, B. Stephens, HVAC filtration for controlling infectious airborne disease transmission in indoor environments: Predicting risk reductions and operational costs, Build. Environ. 70 (2013) 150–160. https://doi.org/10.1016/j.buildenv.2013.08.025.

[31] N.P. Gao, J.L. Niu, M. Perino, P. Heiselberg, The airborne transmission of infection between flats in high-rise residential buildings: Particle simulation, Build. Environ. 44 (2009) 402–410.

[32] Y. Li, S. Duan, I.T.S. Yu, T.W. Wong, Multi-zone modeling of probable SARS virus transmission by airflow between flats in Block E, Amoy Gardens, Indoor Air. 15 (2005) 96–111.

[33] Y. Zhang, G. Feng, Y. Bi, Y. Cai, Z. Zhang, G. Cao, Distribution of droplet aerosols generated by mouth coughing and nose breathing in an air-conditioned room, Sustain. Cities Soc. 51 (2019) 101721. https://doi.org/10.1016/j.scs.2019.101721.

[34] Z.D. Bolashikov, A.K. Melikov, Methods for air cleaning and protection of building occupants from airborne pathogens, Build. Environ. 44 (2009) 1378–1385. https://doi.org/10.1016/j.buildenv.2008.09.001.

[35] World Health Organization, Natural Ventilation for Infection Control in Health-Care Settings, WHO. (2009).

[36] J. Yang, S.C. Sekhar, K.W.D. Cheong, B. Raphael, Performance evaluation of a novel personalized ventilation-personalized exhaust system for airborne infection control, Indoor Air. 25 (2015) 176–187. https://doi.org/10.1111/ina.12127.

[37] A.K. Melikov, Advanced air distribution: Improving health and comfort while reducing energy use, Indoor Air. 26 (2016) 112–124. https://doi.org/10.1111/ina.12206.

[38] A.K. Melikov, Advanced air distribution, ASHRAE J. 53 (2011) 73–77.

[39] D.S. Thatiparti, U. Ghia, K.R. Mead, Assessing effectiveness of ceiling-ventilated mock airborne infection isolation room in preventing Hospital-acquired influenza transmission to health care workers, in: ASHRAE Conf. NIH Public Access, 2016: pp. 35–45.

[40] D.S. Thatiparti, U. Ghia, K.R. Mead, Computational fluid dynamics study on the influence of an alternate ventilation configuration on the possible flow path of infectious cough aerosols in a mock airborne infection isolation room, Sci. Technol. Built Environ. 23 (2017) 355–366. https://doi.org/10.1080/23744731.2016.1222212.

[41] Y. Li, G.M. Leung, J.W. Tang, X. Yang, C.Y.H. Chao, J.Z. Lin, J.W. Lu, P. V. Nielsen, J. Niu, H. Qian, A.C. Sleigh, H.-J.J.J. Su, J. Sundell, T.W. Wong, P.L. Yuen, Role of ventilation in airborne transmission of infectious agents in the built environment - A multidisciplinary systematic review, Indoor Air. 17 (2007) 2–18. https://doi.org/10.1111/j.1600-0668.2006.00445.x.

[42] D. Goncalves, Y. Sheikhnejad, M. Oliveira, N. Martins, One Step Forward Toward Smart City Utopia: Smart Building Energy Management Based on Adaptive Surrogate Modelling, Energy Build. 223 (2020) 110146. https://doi.org/10.1016/j.enbuild.2020.110146.

[43] Y. Sheikhnejad, D. Gonçalves, M. Oliveira, N. Martins, Can buildings be more intelligent than users?- The role of intelligent supervision concept integrated into building predictive control, Energy Reports. 6 (2020) 409–416. https://doi.org/10.1016/j.egyr.2019.08.081.

[44] G. Feng, Y. Zhang, X. Lan, Using CFD method to simulate respiratory aerosols transportation in

ventilated built environment, in: Appl. Mech. Mater., Trans Tech Publications Ltd, 2012: pp. 4292–4297. https://doi.org/10.4028/www.scientific.net/AMM.204-208.4292.

[45] Z. Liu, S. Ma, G. Cao, C. Meng, B.-J. He, Distribution characteristics, growth, reproduction and transmission modes and control strategies for microbial contamination in HVAC systems: A literature review, Energy Build. 177 (2018) 77–95. https://doi.org/10.1016/j.enbuild.2018.07.050.

[46] G. Correia, L. Rodrigues, M. Gameiro da Silva, T. Gonçalves, Airborne route and bad use of ventilation systems as non-negligible factors in SARS-CoV-2 transmission, Med. Hypotheses. 141 (2020). https://doi.org/10.1016/j.mehy.2020.109781.

[47] D. Curseu, M. Popa, D. Sirbu, M.S. Popa, Engineering control of airborne disease transmission in health care facilities, in: IFMBE Proc., Springer, Berlin, Heidelberg, 2009: pp. 1–4. https://doi.org/10.1007/978-3-642-04292-8_1.

[48] C.B. Beggs, K.G. Kerr, C.J. Noakes, E.A. Hathway, P.A. Sleigh, The ventilation of multiple-bed hospital wards: Review and analysis, Am. J. Infect. Control. 36 (2008) 250–259. https://doi.org/10.1016/j.ajic.2007.07.012.

[49] L. Anghel, C.G. Popovici, C. Stătescu, R. Sascău, M. Verdeş, V. Ciocan, I.L. Şerban, M.A. Mărănducă, S.V. Hudişteanu, F.E. Ţurcanu, Impact of hvac-systems on the dispersion of infectious aerosols in a cardiac intensive care unit, Int. J. Environ. Res. Public Health. 17 (2020) 1–17. https://doi.org/10.3390/ijerph17186582.

[50] F. Memarzadeh, W. Xu, Role of air changes per hour (ACH) in possible transmission of airborne infections, Build. Simul. 5 (2012) 15–28. https://doi.org/10.1007/s12273-011-0053-4.

[51] N.P. Gao, J.L. Niu, Modeling particle dispersion and deposition in indoor environments, Atmos. Environ. 41 (2007) 3862–3876. https://doi.org/10.1016/j.atmosenv.2007.01.016.

[52] Z. Kang, Y. Zhang, H. Fan, G. Feng, Numerical Simulation of Coughed Droplets in the Air-Conditioning Room, Procedia Eng. 121 (2015) 114–121. https://doi.org/10.1016/j.proeng.2015.08.1031.

[53] G. Feng, Y. Zhang, X. Lan, Numerical study of the respiratory aerosols transportation in ventilated classroom, in: Appl. Mech. Mater., Trans Tech Publications Ltd, 2012: pp. 4298–4304. https://doi.org/10.4028/www.scientific.net/AMM.204-208.4298.

[54] S. Jacob, S.S. Yadav, B.S. Sikarwar, Design and simulation of isolation room for a hospital, in: Lect. Notes Mech. Eng., Pleiades Publishing, 2019: pp. 75–93. https://doi.org/10.1007/978-981-13-6416-7_8.

[55] R. Mead-Hunter, B.J. Mullins, A.J.C. King, Development and validation of a computational fluid dynamics (CFD) solver for droplet-fibre systems, in: MODSIM 2011 - 19th Int. Congr. Model. Simul. - Sustain. Our Futur. Underst. Living with Uncertain., Modelling and Simulation Society of Australia and New Zealand Inc, 2011: pp. 572–578. https://doi.org/10.36334/modsim.2011.a7.mead_hunter.

[56] L. Morawska, J.W. Tang, W. Bahnfleth, P.M. Bluyssen, A. Boerstra, G. Buonanno, J. Cao, S. Dancer, A. Floto, F. Franchimon, C. Haworth, J. Hogeling, C. Isaxon, J.L. Jimenez, J. Kurnitski, Y. Li, M. Loomans, G. Marks, L.C. Marr, L. Mazzarella, A.K. Melikov, S. Miller, D.K. Milton, W. Nazaroff, P. V. Nielsen, C. Noakes, J. Peccia, X. Querol, C. Sekhar, O. Seppänen, S. ichi Tanabe, R. Tellier, K.W. Tham, P. Wargocki, A. Wierzbicka, M. Yao, How can airborne transmission of COVID-19 indoors be minimised?, Environ. Int. 142 (2020) 105832.

https://doi.org/10.1016/j.envint.2020.105832.

[57] Y.H. Yau, D. Chandrasegaran, A. Badarudin, The ventilation of multiple-bed hospital wards in the tropics: A review, Build. Environ. 46 (2011) 1125–1132. https://doi.org/10.1016/j.buildenv.2010.11.013.

[58] A. Baumann, D. Hoch, J. Behringer, J. Niessner, Macro-scale modeling and simulation of two-phase flow in fibrous liquid aerosol filters, Eng. Appl. Comput. Fluid Mech. 14 (2020) 1325–1336. https://doi.org/10.1080/19942060.2020.1828174.

[59] S. Fotovati, H. Vahedi Tafreshi, B. Pourdeyhimi, Influence of fiber orientation distribution on performance of aerosol filtration media, Chem. Eng. Sci. 65 (2010) 5285–5293. https://doi.org/10.1016/j.ces.2010.06.032.

[60] R. Mead-Hunter, A.J.C. King, G. Kasper, B.J. Mullins, Computational fluid dynamics (CFD) simulation of liquid aerosol coalescing filters, J. Aerosol Sci. 61 (2013) 36–49. https://doi.org/10.1016/j.jaerosci.2013.03.009.

[61] M.P. Wan, C.Y.H. Chao, Transport characteristics of expiratory droplets and droplet nuclei in indoor environments with different ventilation airflow patterns, J. Biomech. Eng. 129 (2007) 341–353. https://doi.org/10.1115/1.2720911.

[62] F. Atci, Y.E. Cetin, M. Avci, O. Aydin, Evaluation of in-duct UV-C lamp array on air disinfection: A numerical analysis, Sci. Technol. Built Environ. 27 (2020) 98–108. https://doi.org/10.1080/23744731.2020.1776549.

[63] A.R. Escombe, D.A.J. Moore, R.H. Gilman, M. Navincopa, E. Ticona, B. Mitchell, C. Noakes, C. Martinez, P. Sheen, R. Ramirez, W. Quino, A. Gonzalez, J.S. Friedland, C.A. Evans, Upper-room ultraviolet light and negative air ionization to prevent tuberculosis transmissio, PLoS Med. 6 (2009) 0312–0323. https://doi.org/10.1371/journal.pmed.1000043.

[64] A.A. Aliabadi, S.N. Rogak, K.H. Bartlett, S.I. Green, Preventing Airborne Disease Transmission: Review of Methods for Ventilation Design in Health Care Facilities, Adv. Prev. Med. 2011 (2011) 1–21. https://doi.org/10.4061/2011/124064.

[65] A. Fernstrom, M. Goldblatt, Aerobiology and Its Role in the Transmission of Infectious Diseases, J. Pathog. 2013 (2013) 1–13. https://doi.org/10.1155/2013/493960.

[66] J.E. Allen, J.J. Close, D.L. Henshaw, Static electric fields as a mediator of hospital infection, in: Indoor Built Environ., Sage PublicationsSage CA: Thousand Oaks, CA, 2006: pp. 49–52. https://doi.org/10.1177/1420326X06061502.

[67] D.A. Cozanitis, J. Ojajärvi, P. Mäkelä, Antistatic treatment for reducing airborne contamination of insulating materials in intensive care, Acta Anaesthesiol. Scand. 32 (1988) 343–346. https://doi.org/10.1111/j.1399-6576.1988.tb02741.x.

[68] H. Destaillats, R.L. Maddalena, B.C. Singer, A.T. Hodgson, T.E. McKone, Indoor pollutants emitted by office equipment: A review of reported data and information needs, Atmos. Environ. 42 (2008) 1371–1388. https://doi.org/10.1016/j.atmosenv.2007.10.080.

[69] A.G. Buchan, L. Yang, K.D. Atkinson, Predicting airborne coronavirus inactivation by far-UVC in populated rooms using a high-fidelity coupled radiation-CFD model, Sci. Rep. 10 (2020). https://doi.org/10.1038/s41598-020-76597-y.

[70] S. He, J. Han, Electrostatic fine particles emitted from laser printers as potential vectors for airborne transmission of COVID-19, Environ. Chem. Lett. (2020).

https://doi.org/10.1007/s10311-020-01069-8.

[71] C.J. Noakes, P.A. Sleigh, L.A. Fletcher, C.B. Beggs, Use of CFD modelling to optimise the design of upper-room UVGI disinfection systems for ventilated rooms, Indoor Built Environ. 15 (2006) 347–356. https://doi.org/10.1177/1420326X06067353.

[72] Z. Feng, W. Pan, H. Zhang, X. Cheng, Z. Long, J. Mo, Evaluation of the performance of an electrostatic enhanced air filter (EEAF) by a numerical method, Powder Technol. 327 (2018) 201–214.

[73] Z. Feng, S.-J. Cao, J. Wang, P. Kumar, F. Haghighat, Indoor airborne disinfection with electrostatic disinfector (ESD): Numerical simulations of ESD performance and reduction of computing time, Build. Environ. 200 (2021) 107956.

[74] W. Lu, A.T. Howarth, N. Adam, S.B. Riffati, Modelling and measurement of airflow and aerosol particle distribution in a ventilated two-zone chamber, Build. Environ. 31 (1996) 417–423. https://doi.org/10.1016/0360-1323(96)00019-4.

[75] C.H. Cheong, S. Lee, Case study of airborne pathogen dispersion patterns in emergency departments with different ventilation and partition conditions, Int. J. Environ. Res. Public Health. 15 (2018). https://doi.org/10.3390/ijerph15030510.

[76] A. Sopeyin, E. Hornsey, T. Okwor, Y. Alimi, T. Raji, A. Mohammed, H. Moges, E.V.C. Onwuekwe, F.J. Minja, G. Gon, O. Ogbuagu, F. Ogunsola, E. Paintsil, Transmission risk of respiratory viruses in natural and mechanical ventilation environments: Implications for SARS-CoV-2 transmission in Africa, BMJ Glob. Heal. 5 (2020) 3522. https://doi.org/10.1136/bmjgh-2020-003522.

[77] H. Qian, Y. Li, W.H. Seto, P. Ching, W.H. Ching, H.Q. Sun, Natural ventilation for reducing airborne infection in hospitals, Build. Environ. 45 (2010) 559–565. https://doi.org/10.1016/j.buildenv.2009.07.011.

[78] A.R. Escombe, C.C. Oeser, R.H. Gilman, M. Navincopa, E. Ticona, W. Pan, C. Martínez, J. Chacaltana, R. Rodríguez, D.A.J. Moore, J.S. Friedland, C.A. Evans, Natural ventilation for the prevention of airborne contagion, PLoS Med. 4 (2007) 0309–0317. https://doi.org/10.1371/journal.pmed.0040068.

[79] X. Liu, J. Niu, M. Perino, P. Heiselberg, Numerical simulation of inter-flat air cross-contamination under the condition of single-sided natural ventilation, J. Build. Perform. Simul. 1 (2008) 133–147. https://doi.org/10.1080/19401490802250462.

[80] H. Motamedi, M. Shirzadi, Y. Tominaga, P.A. Mirzaei, CFD Modeling of Airborne pathogen transmission of COVID19 in confined spaces under Different Ventilation Strategies, Sustain. Cities Soc. (2021) 103397.

[81] A. Konda, A. Prakash, G.A. Moss, M. Schmoldt, G.D. Grant, S. Guha, Aerosol Filtration Efficiency of Common Fabrics Used in Respiratory Cloth Masks, ACS Nano. 14 (2020) 6339–6347. https://doi.org/10.1021/acsnano.0c03252.

[82] R. Mittal, C. Meneveau, W. Wu, A mathematical framework for estimating risk of airborne transmission of COVID-19 with application to face mask use and social distancing, Phys. Fluids. 32 (2020). https://doi.org/10.1063/5.0025476.

[83] W.G. Lindsley, J.D. Noti, F.M. Blachere, J. V. Szalajda, D.H. Beezhold, Efficacy of face shields against cough aerosol droplets from a cough simulator, J. Occup. Environ. Hyg. 11 (2014) 509–518. https://doi.org/10.1080/15459624.2013.877591.

[84]   J. Wei, Y. Li, Airborne spread of infectious agents in the indoor environment, Am. J. Infect. Control. 44 (2016) S102–S108. https://doi.org/10.1016/j.ajic.2016.06.003.

[85]   D.K. Chu, E.A. Akl, S. Duda, K. Solo, S. Yaacoub, H.J. Schünemann, A. El-harakeh, A. Bognanni, T. Lotfi, M. Loeb, A. Hajizadeh, A. Bak, A. Izcovich, C.A. Cuello-Garcia, C. Chen, D.J. Harris, E. Borowiack, F. Chamseddine, F. Schünemann, G.P. Morgano, G.E.U. Muti Schünemann, G. Chen, H. Zhao, I. Neumann, J. Chan, J. Khabsa, L. Hneiny, L. Harrison, M. Smith, N. Rizk, P. Giorgi Rossi, P. AbiHanna, R. El-khoury, R. Stalteri, T. Baldeh, T. Piggott, Y. Zhang, Z. Saad, A. Khamis, M. Reinap, Physical distancing, face masks, and eye protection to prevent person-to-person transmission of SARS-CoV-2 and COVID-19: a systematic review and meta-analysis, Lancet. 395 (2020) 1973–1987. https://doi.org/10.1016/S0140-6736(20)31142-9.

[86]   M. Rahiminejad, A. Haghighi, A. Dastan, O. Abouali, M. Farid, G. Ahmadi, Computer simulations of pressure and velocity fields in a human upper airway during sneezing, Comput. Biol. Med. 71 (2016) 115–127. https://doi.org/10.1016/j.compbiomed.2016.01.022.

[87]   V. Kumar, S. Nallamothu, S. Shrivastava, H. Jadeja, P. Nakod, P. Andrade, P. Doshi, G. Kumaraswamy, On the utility of cloth facemasks for controlling ejecta during respiratory events, ArXiv. (2020).

[88]   M.R. Pendar, J.C. Páscoa, Numerical modeling of the distribution of virus carrying saliva droplets during sneeze and cough, Phys. Fluids. 32 (2020) 083305. https://doi.org/10.1063/5.0018432.

[89]   H. Arjmandi, R. Amini, F. Khani, M. Fallahpour, Minimizing the respiratory pathogen transmission: numerical study and multi-objective optimization of ventilation systems in a classroom, Therm. Sci. Eng. Prog. (2021) 101052. https://doi.org/10.1016/j.tsep.2021.101052.

[90]   M. Jayaweera, H. Perera, B. Gunawardana, J. Manatunge, Transmission of COVID-19 virus by droplets and aerosols: A critical review on the unresolved dichotomy, Environ. Res. 188 (2020). https://doi.org/10.1016/j.envres.2020.109819.

[91]   S.W. Zhu, S. Kato, J.H. Yang, Study on transport characteristics of saliva droplets produced by coughing in a calm indoor environment, Build. Environ. 41 (2006) 1691–1702. https://doi.org/10.1016/j.buildenv.2005.06.024.

[92]   J.K. Gupta, C.H. Lin, Q. Chen, Flow dynamics and characterization of a cough, Indoor Air. 19 (2009) 517–525. https://doi.org/10.1111/j.1600-0668.2009.00619.x.

[93]   N.P. Gao, J.L. Niu, M. Perino, P. Heiselberg, The airborne transmission of infection between flats in high-rise residential buildings: Tracer gas simulation, Build. Environ. 43 (2008) 1805–1817. https://doi.org/10.1016/j.buildenv.2007.10.023.

[94]   Z. Zhang, W. Zhang, Z.J. Zhai, Q.Y. Chen, Evaluation of various turbulence models in predicting airflow and turbulence in enclosed environments by CFD: Part 2—comparison with experimental data from literature, HVAC R Res. 13 (2007) 871–886. https://doi.org/10.1080/10789669.2007.10391460.

[95]   B.E. Launder, B.I. Sharma, Application of the energy-dissipation model of turbulence to the calculation of flow near a spinning disc, Lett. Heat Mass Transf. 1 (1974) 131–137. https://doi.org/10.1016/0094-4548(74)90150-7.

[96]   S. Peng, Q. Chen, E. Liu, Corrigendum to "The role of computational fluid dynamics tools on investigation of pathogen transmission: Prevention and control" [Sci. Total Environ. 746 (2020) 142090] (Science of the Total Environment (2020) 746, (S0048969720356199),

(10.1016/j.scitote, Sci. Total Environ. 764 (2021) 142862.
https://doi.org/10.1016/j.scitotenv.2020.142862.

[97] V. D'Alessandro, M. Falone, L. Giammichele, R. Ricci, Eulerian-Lagrangian modeling of cough droplets irradiated by ultraviolet-C light in relation to SARS-CoV-2 transmission, Phys. Fluids. 33 (2021). https://doi.org/10.1063/5.0039224.

[98] P.W. Longest, J. Xi, Effectiveness of direct Lagrangian tracking models for simulating nanoparticle deposition in the upper airways, Aerosol Sci. Technol. 41 (2007) 380–397. https://doi.org/10.1080/02786820701203223.

[99] L. Pichelstorfer, R. Winkler-Heil, W. Hofmann, Lagrangian/Eulerian model of coagulation and deposition of inhaled particles in the human lung, J. Aerosol Sci. 64 (2013) 125–142. https://doi.org/10.1016/j.jaerosci.2013.05.007.

[100] R. Kannan, P. Guo, A. Przekwas, Particle transport in the human respiratory tract: formulation of a nodal inverse distance weighted Eulerian–Lagrangian transport and implementation of the Wind–Kessel algorithm for an oral delivery, Int J Numer Method Biomed Eng. 32 (2016). https://doi.org/https://doi.org/10.1002/cnm.2746.

[101] Mohammad Moshfeghi, N. Hur, Investigation on the effects of different ventilation scenarios on spread patterns and risk factor of COVID-19 virus in indoor spaces, in: 8th Asian Symp. Comput. Heat Transf. Fluid Flow, Qingdao, 2021.

[102] Z. Zhang, Q. Chen, Comparison of the Eulerian and Lagrangian methods for predicting particle transport in enclosed spaces, Atmos. Environ. 41 (2007) 5236–5248. https://doi.org/10.1016/j.atmosenv.2006.05.086.

[103] P.A. Mirzaei, M. Moshfeghi, H. Motamedi, Y. Sheikhnejad, H. Bordbar, A simplified tempo-spatial model to predict airborne pathogen release risk in enclosed spaces: An Eulerian-Lagrangian CFD approach, Build. Environ. 207 (2022) 108428. https://doi.org/10.1016/j.buildenv.2021.108428.

[104] B.S. Cohen, B. Asgharian, Deposition of ultrafine particles in the upper airways: An empirical analysis, J. Aerosol Sci. 21 (1990) 789–797. https://doi.org/10.1016/0021-8502(90)90044-X.

[105] P.W. Longest, J. Xi, Computational investigation of particle inertia effects on submicron aerosol deposition in the respiratory tract, J. Aerosol Sci. 38 (2007) 111–130. https://doi.org/10.1016/j.jaerosci.2006.09.007.

[106] J. Dombard, G. Iaccarino, Sensitivity analysis to the normal grid-resolution in a turbulent channel flow using large-eddy simulations, Cent. Turbul. Res. Annu. Res. Briefs. (2012) 265–274.

[107] P.R. Spalart, Detached-eddy simulation, Annu. Rev. Fluid Mech. 41 (2009) 181–202. https://doi.org/10.1146/annurev.fluid.010908.165130.

[108] H. Pitsch, Large-eddy simulation of turbulent combustion, Annu. Rev. Fluid Mech. 38 (2006) 453–482. https://doi.org/10.1146/annurev.fluid.38.050304.092133.

[109] R.O. Fox, Large-eddy-simulation tools for multiphase flows, Annu. Rev. Fluid Mech. 44 (2011) 47–76. https://doi.org/10.1146/annurev-fluid-120710-101118.

[110] A.H. Shafaghi, F.R. Talabazar, A. Koşar, M. Ghorbani, on the effect of the respiratory droplet generation condition on COVID-19 transmission, Fluids. (2020). https://doi.org/10.3390/fluids5030113.

[111] C.K. Ho, Modeling airborne pathogen transport and transmission risks of SARS-CoV-2, Appl. Math. Model. 95 (2021) 297–319. https://doi.org/10.1016/j.apm.2021.02.018.

[112] S.P. Domino, A Case Study on Pathogen Transport, Deposition, Evaporation and Transmission: Linking High-Fidelity Computational Fluid Dynamics Simulations to Probability of Infection, Int. J. Comut. Fluid Dyn. (2021). https://doi.org/10.1080/10618562.2021.1905801.

[113] H.M. Zoka, M. Moshfeghi, H. Bordbar, P.A. Mirzaei, Y. Sheikhnejad, A cfd approach for risk assessment based on airborne pathogen transmission, Atmosphere (Basel). 12 (2021) 1–27. https://doi.org/10.3390/atmos12080986.

[114] E.A. Hathway, C.J. Noakes, P.A. Sleigh, L.A. Fletcher, CFD simulation of airborne pathogen transport due to human activities, Build. Environ. 46 (2011) 2500–2511. https://doi.org/10.1016/j.buildenv.2011.06.001.

[115] E.A. Hathway, CFD Modelling of Pathogen Transport due to Human Activity, University of Leeds, 2008. https://etheses.whiterose.ac.uk/11284/.

[116] A. Muhammad, R. Pendyala, N. Rahmanian, CFD simulation of droplet formation under various parameters in prilling process, Appl. Mech. Mater. 625 (2014) 394–397. https://doi.org/10.4028/www.scientific.net/AMM.625.394.

[117] M. Karimi, R. Andersson, Stochastic simulation of droplet breakup in turbulence, Chem. Eng. J. 380 (2020) 122502. https://doi.org/10.1016/j.cej.2019.122502.

[118] S. Chadha, R. Jefferson-Loveday, T. Hussain, A high-fidelity simulation of the primary breakup within suspension high velocity oxy fuel thermal spray using a coupled volume of fluid and discrete phase model, Int. J. Multiph. Flow. 133 (2020) 103445. https://doi.org/10.1016/j.ijmultiphaseflow.2020.103445.

[119] G. Strotos, I. Malgarinos, N. Nikolopoulos, M. Gavaises, Predicting droplet deformation and breakup for moderate Weber numbers, Int. J. Multiph. Flow. 85 (2016) 96–109. https://doi.org/10.1016/j.ijmultiphaseflow.2016.06.001.

[120] M. Dai, D.P. Schmidt, Numerical simulation of head-on droplet collision: Effect of viscosity on maximum deformation, Phys. Fluids. 17 (2005) 1–5. https://doi.org/10.1063/1.1874232.

[121] A. Munnannur, R.D. Reitz, A new predictive model for fragmenting and non-fragmenting binary droplet collisions, Int. J. Multiph. Flow. 33 (2007) 873–896. https://doi.org/10.1016/j.ijmultiphaseflow.2007.03.003.

[122] C. Planchette, H. Hinterbichler, M. Liu, D. Bothe, G. Brenn, Colliding drops as coalescing and fragmenting liquid springs, J. Fluid Mech. 814 (2017) 277–300. https://doi.org/10.1017/jfm.2016.852.

[123] G. Finotello, J.T. Padding, N.G. Deen, A. Jongsma, F. Innings, J.A.M. Kuipers, Effect of viscosity on droplet-droplet collisional interaction, Phys. Fluids. 29 (2017). https://doi.org/10.1063/1.4984081.

[124] G. Finotello, R.F. Kooiman, J.T. Padding, K.A. Buist, A. Jongsma, F. Innings, J.A.M. Kuipers, The dynamics of milk droplet–droplet collisions, Exp. Fluids. 59 (2018) 1–19. https://doi.org/10.1007/s00348-017-2471-2.

[125] A. Acevedo-Malavé, M. Garca-Sucre, Coalescence collision of liquid drops I: Off-center collisions of equal-size drops, AIP Adv. 1 (2011). https://doi.org/10.1063/1.3624553.

[126] A. Acevedo-Malavé, Hydrodynamics coalescence collision of three liquid drops in 3D with smoothed particle hydrodynamics, AIP Adv. 2 (2012). https://doi.org/10.1063/1.4757966.

[127] H. Zhao, Z.W. Wu, W.F. Li, J.L. Xu, H.F. Liu, Interaction of two drops in the bag breakup regime by a continuous air jet, Fuel. 236 (2019) 843–850. https://doi.org/10.1016/j.fuel.2018.09.067.

[128] A. Agarwal, Y. Wang, L. Liang, C. Naik, The Computational Cost and Accuracy of Spray Droplet Collision Models, SAE Tech. (2019). https://doi.org/https://doi.org/10.4271/2019-01-0279.

[129] L. Zhou, L. Zhang, L. Bai, W. Shi, W. Li, C. Wang, R. Agarwal, Experimental study and transient CFD/DEM simulation in a fluidized bed based on different drag models, RSC Adv. 7 (2017) 12764–12774. https://doi.org/10.1039/c6ra28615a.

[130] L. Lu, S. Benyahia, T. Li, An efficient and reliable predictive method for fluidized bed simulation, AIChE J. 63 (2017) 5320–5334. https://doi.org/10.1002/aic.15832.

[131] X. Xie, Y. Li, A.T.Y. Chwang, P.L. Ho, W.H. Seto, How far droplets can move in indoor environments - revisiting the Wells evaporation-falling curve, Indoor Air. 17 (2007) 211–225. https://doi.org/10.1111/j.1600-0668.2007.00469.x.

[132] T. Zhang, Study on Surface Tension and Evaporation Rate of Human Saliva, Saline, and Water Droplets, Grad. Theses, Diss. Probl. Reports. (2011). https://researchrepository.wvu.edu/etd/2271.

[133] S. Chaudhuri, S. Basu, P. Kabi, V.R. Unni, A. Saha, Modeling the role of respiratory droplets in Covid-19 type pandemics, Phys. Fluids. 32 (2020). https://doi.org/10.1063/5.0015984.

[134] V. Stadnytskyi, C.E. Bax, A. Bax, P. Anfinrud, The airborne lifetime of small speech droplets and their potential importance in SARS-CoV-2 transmission, Proc. Natl. Acad. Sci. U. S. A. 117 (2020) 11875–11877. https://doi.org/10.1073/pnas.2006874117.

[135] A.A. Aliabadi, S.N. Rogak, S.I. Green, K.H. Bartlett, CFD simulation of human coughs and sneezes: A study in droplet dispersion, heat, and mass transfer, ASME Int. Mech. Eng. Congr. Expo. Proc. 7 (2010) 1051–1060. https://doi.org/10.1115/IMECE2010-37331.

[136] X. Li, Y. Shang, Y. Yan, L. Yang, J. Tu, Modelling of evaporation of cough droplets in inhomogeneous humidity fields using the multi-component Eulerian-Lagrangian approach, Build. Environ. 128 (2018) 68–76. https://doi.org/10.1016/j.buildenv.2017.11.025.

[137] J. Redrow, S. Mao, I. Celik, J.A. Posada, Z. gang Feng, Modeling the evaporation and dispersion of airborne sputum droplets expelled from a human cough, Build. Environ. 46 (2011) 2042–2051. https://doi.org/10.1016/j.buildenv.2011.04.011.

[138] G. Busco, S.R. Yang, J. Seo, Y.A. Hassan, Sneezing and asymptomatic virus transmission, Phys. Fluids. 32 (2020). https://doi.org/10.1063/5.0019090.

[139] M. Zhou, J. Zou, A dynamical overview of droplets in the transmission of respiratory infectious diseases, Phys. Fluids. 33 (2021). https://doi.org/10.1063/5.0039487.

[140] K. Mahjoub Mohammed Merghani, B. Sagot, E. Gehin, G. Da, C. Motzkus, A review on the applied techniques of exhaled airflow and droplets characterization, Indoor Air. 31 (2021) 7–25. https://doi.org/10.1111/ina.12770.

[141] J.W. Tang, C.J. Noakes, P. V. Nielsen, I. Eames, A. Nicolle, Y. Li, G.S. Settles, Observing and

quantifying airflows in the infection control of aerosol- and airborne-transmitted diseases: An overview of approaches, J. Hosp. Infect. 77 (2011) 213–222. https://doi.org/10.1016/j.jhin.2010.09.037.

[142] J. Elcner, F. Lizal, J. Jedelsky, M. Jicha, M. Chovancova, Numerical investigation of inspiratory airflow in a realistic model of the human tracheobronchial airways and a comparison with experimental results, Biomech. Model. Mechanobiol. 15 (2016) 447–469. https://doi.org/10.1007/s10237-015-0701-1.

[143] L. Feng, S. Yao, H. Sun, N. Jiang, J. Liu, TR-PIV measurement of exhaled flow using a breathing thermal manikin, Build. Environ. 94 (2015) 683–693. https://doi.org/10.1016/j.buildenv.2015.11.001.

[144] Z.J. Marr D, Khan T, Glauser M, Higuchi H, On particle image velocimetry (PIV) measurements in the breathing zone of a thermal breathing mannequin, ASHRAE Trans. 111 (2005) 299–305.

[145] S.B. Kwon, J. Park, J. Jang, Y. Cho, D.S. Park, C. Kim, G.N. Bae, A. Jang, Study on the initial velocity distribution of exhaled air from coughing and speaking, Chemosphere. 87 (2012) 1260–1264. https://doi.org/10.1016/j.chemosphere.2012.01.032.

[146] X. Xu, J. Wu, W. Weng, M. Fu, Investigation of inhalation and exhalation flow pattern in a realistic human upper airway model by PIV experiments and CFD simulations, Biomech. Model. Mechanobiol. 19 (2020) 1679–1695. https://doi.org/10.1007/s10237-020-01299-3.

[147] N. Dudalski, Experimental measurements of human cough airflows from healthy subjects and those infected with respiratory viruses, University of Western Ontario, 2019.

[148] W. Sun, J. Ji, Transport of droplets expelled by coughing in ventilated rooms, Indoor Built Environ. 16 (2007) 493–504. https://doi.org/10.1177/1420326X07084290.

[149] L. Bourouiba, E. Dehandschoewercker, J.W.M. Bush, Violent expiratory events: On coughing and sneezing, J. Fluid Mech. 745 (2014) 537–563. https://doi.org/10.1017/jfm.2014.88.

[150] S. Liu, A. Novoselac, Transport of airborne particles from an unobstructed cough jet, Aerosol Sci. Technol. 48 (2014) 1183–1194. https://doi.org/10.1080/02786826.2014.968655.

[151] W. Lindsley, J.S. Reynolds, J. V. Szalajda, J.D. Noti, D.H. Beezhold, A Cough Aerosol Simulator for the Study of Disease Transmission by Human Cough-Generated Aerosols, Aerosol Sci. Technol. 47 (2013) 937–944. https://doi.org/10.1080/02786826.2013.803019.

[152] J. Wei, Y. Li, Human cough as a two-stage jet and its role in particle transport, PLoS One. 12 (2017) 1–15. https://doi.org/10.1371/journal.pone.0169235.

[153] J.B. Day, B.M. Jones, A.A. Afshari, D.G. Frazer, W.T. Goldsmith, Temporal Characteristics Of Aerosol Generation During A Voluntary Cough, in: Airw. Funct. AEROSOLS Child. ADULTS MICE, American Thoracic Society, New Orleans, LA USA, 2010: pp. A2183–A2183. https://doi.org/10.1164/ajrccm-conference.2010.181.1_meetingabstracts.a2183.

[154] B. Sokoray-Varga, J. Józsa, Particle tracking velocimetry (PTV) and its application to analyse free surface flows in laboratory scale models, Period. Polytech. Civ. Eng. 52 (2008) 63–71. https://doi.org/10.3311/pp.ci.2008-2.02.

[155] T. Janke, R. Schwarze, K. Bauer, PIV-PTV comparison of the oscillating flow inside the human lungs, 13th Int. Symp. Part. Image Velocim. (2019) 232–238.

[156] P. Bahl, C.M. de Silva, A.A. Chughtai, C.R. MacIntyre, C. Doolan, An experimental framework

to capture the flow dynamics of droplets expelled by a sneeze, Exp. Fluids. 61 (2020) 1–9. https://doi.org/10.1007/s00348-020-03008-3.

[157] C.Y.H. Chao, M.P. Wan, L. Morawska, G.R. Johnson, Z.D. Ristovski, M. Hargreaves, K. Mengersen, S. Corbett, Y. Li, X. Xie, D. Katoshevski, Characterization of expiration air jets and droplet size distributions immediately at the mouth opening, J. Aerosol Sci. 40 (2009) 122–133. https://doi.org/10.1016/j.jaerosci.2008.10.003.

[158] L. Stabile, F. Arpino, G. Buonanno, A. Russi, A. Frattolillo, A simplified benchmark of ultrafine particle dispersion in idealized urban street canyons: A wind tunnel study, Build. Environ. 93 (2015) 186–198. https://doi.org/10.1016/j.buildenv.2015.05.045.

[159] A. Khosronejad, C. Santoni, K. Flora, Z. Zhang, S. Kang, S. Payabvash, F. Sotiropoulos, Fluid dynamics simulations show that facial masks can suppress the spread of COVID-19 in indoor environments., ArXiv. 125109 (2020). https://doi.org/10.1063/5.0035414.

[160] G. Buonanno, A.A. Lall, L. Stabile, Temporal size distribution and concentration of particles near a major highway, Atmos. Environ. 43 (2009) 1100–1105. https://doi.org/10.1016/j.atmosenv.2008.11.011.

[161] S. Ren, W. Li, L. Wang, Y. Shi, M. Cai, L. Hao, Z. Luo, J. Niu, W. Xu, Z. Luo, Numerical Analysis of Airway Mucus Clearance Effectiveness Using Assisted Coughing Techniques, Sci. Rep. 10 (2020) 1–10. https://doi.org/10.1038/s41598-020-58922-7.

[162] J.W. Tang, T.J. Liebner, B.A. Craven, G.S. Settles, A schlieren optical study of the human cough with and without wearing masks for aerosol infection control, J. R. Soc. Interface. 6 (2009) 727–736. https://doi.org/10.1098/rsif.2009.0295.focus.

[163] J.M. Villafruela, I. Olmedo, M. Ruiz de Adana, C. Méndez, P. V. Nielsen, CFD analysis of the human exhalation flow using different boundary conditions and ventilation strategies, Build. Environ. 62 (2013) 191–200. https://doi.org/10.1016/j.buildenv.2013.01.022.

[164] G. Zayas, M.C. Chiang, E. Wong, F. MacDonald, C.F. Lange, A. Senthilselvan, M. King, Cough aerosol in healthy participants: Fundamental knowledge to optimize droplet-spread infectious respiratory disease management, BMC Pulm. Med. 12 (2012). https://doi.org/10.1186/1471-2466-12-11.

[165] X. Li, Y. Yan, J. Tu, The simplification of computer simulated persons (CSPs) in CFD models of occupied indoor spaces, Build. Environ. 93 (2015) 155–164. https://doi.org/10.1016/j.buildenv.2015.06.014.

[166] Y. Yan, X. Li, L. Yang, J. Tu, Evaluation of manikin simplification methods for CFD simulations in occupied indoor environments, Energy Build. 127 (2016) 611–626. https://doi.org/10.1016/j.enbuild.2016.06.030.

[167] J.K. Gupta, C.H. Lin, Q. Chen, Characterizing exhaled airflow from breathing and talking, Indoor Air. 20 (2010) 31–39. https://doi.org/10.1111/j.1600-0668.2009.00623.x.

[168] W. Villasmil, L.J. Fischer, J. Worlitschek, A review and evaluation of thermal insulation materials and methods for thermal energy storage systems, Renew. Sustain. Energy Rev. 103 (2019) 71–84. https://doi.org/10.1016/j.rser.2018.12.040.

[169] F.A. Berlanga, L. Liu, P. V. Nielsen, R.L. Jensen, A. Costa, I. Olmedo, M.R. de Adana, Influence of the geometry of the airways on the characterization of exhalation flows. Comparison between two different airway complexity levels performing two different breathing functions, Sustain. Cities Soc. 53 (2020). https://doi.org/10.1016/j.scs.2019.101874.

[170] J.W. Tang, A.D. Nicolle, C.A. Klettner, J. Pantelic, L. Wang, A. Bin Suhaimi, A.Y.L. Tan, G.W.X. Ong, R. Su, C. Sekhar, D.D.W. Cheong, K.W. Tham, Airflow Dynamics of Human Jets: Sneezing and Breathing - Potential Sources of Infectious Aerosols, PLoS One. 8 (2013) 1–7. https://doi.org/10.1371/journal.pone.0059970.

[171] M.W. Jennison, H.E. Edgerton, Droplet infection of air; high-speed photography of droplet production by sneezing, Proc. Soc. Exp. Biol. Med. (1940) 455–458.

[172] H. Mortazavy Beni, K. Hassani, S. Khorramymehr, Study of the sneezing effects on the real human upper airway using fluid–structure interaction method, J. Brazilian Soc. Mech. Sci. Eng. 41 (2019) 1–13. https://doi.org/10.1007/s40430-019-1677-z.

[173] H. Mortazavy beni, K. Hassani, S. Khorramymehr, In silico investigation of sneezing in a full real human upper airway using computational fluid dynamics method, Comput. Methods Programs Biomed. 177 (2019) 203–209. https://doi.org/10.1016/j.cmpb.2019.05.031.

[174] W.F. Wells, Airborne Contagion and Air Hygiene: an Ecological Study of Droplet Infection, Harvard University Press, MACambridge, 1955.

[175] H. Zhang, D. Li, L. Xie, Y. Xiao, Documentary Research of Human Respiratory Droplet Characteristics, Procedia Eng. 121 (2015) 1365–1374. https://doi.org/10.1016/j.proeng.2015.09.023.

[176] T. Dbouk, D. Drikakis, On coughing and airborne droplet transmission to humans, Phys. Fluids. 32 (2020). https://doi.org/10.1063/5.0011960.

[177] A.C. Almstrand, M. Josefson, A. Bredberg, J. Lausmaa, P. Sjövall, P. Larsson, A.C. Olin, TOF-SIMS analysis of exhaled particles from patients with asthma and healthy controls, Eur. Respir. J. 39 (2012) 59–66. https://doi.org/10.1183/09031936.00195610.

[178] N.J. Greening, P. Larsson, E. Ljungström, S. Siddiqui, A.C. Olin, Small droplet emission in exhaled breath during different breathing manoeuvres: Implications for clinical lung function testing during COVID-19, Allergy Eur. J. Allergy Clin. Immunol. (2020) 1–3. https://doi.org/10.1111/all.14596.

[179] M. Alsved, A. Matamis, R. Bohlin, M. Richter, P.E. Bengtsson, C.J. Fraenkel, P. Medstrand, J. Löndahl, Exhaled respiratory particles during singing and talking, Aerosol Sci. Technol. 54 (2020) 1245–1248. https://doi.org/10.1080/02786826.2020.1812502.

[180] G.H. Wan, C.L. Wu, Y.F. Chen, S.H. Huang, Y.L. Wang, C.W. Chen, Particle size concentration distribution and influences on exhaled breath particles in mechanically ventilated patients, PLoS One. 9 (2014) 0–8. https://doi.org/10.1371/journal.pone.0087088.

[181] J. Lee, V.H. Chu, TURBULENT JETSAND PLUMES - A LAGRANGIAN APPROACH, Springer Science+Business Media, New York, USA, 2003. https://doi.org/10.1007/978-1-4615-0407-8.

[182] M. Versluis, High-speed imaging in fluids, Exp. Fluids. 54 (2013). https://doi.org/10.1007/s00348-013-1458-x.

[183] J.D. Anderson, Fundamentals of Aerodynamics, 6th ed., McGraw-Hill, New York, USA, 2017.

[184] Euler and Lagrange, Vis. Room. (2020). http://www.thevisualroom.com/18_cfd_notes/01_fluid_mechanics_and_heat_transfer/07_euler_and_lagrange.html#:~:text=¶-,Lagrange%3A,particles in a flow field.

[185] J. Price, Lagrangian-Eulerian Fluid Representation of Fluid Flow, Lect. Notes. (2006) 1–91.

[186] J.M. Qiu, C.W. Shu, Positivity preserving semi-Lagrangian discontinuous Galerkin formulation: Theoretical analysis and application to the Vlasov-Poisson system, J. Comput. Phys. 230 (2011) 8386–8409. https://doi.org/10.1016/j.jcp.2011.07.018.

[187] J. Kitscha, G. Kocamustafaogullari, Breakup criteria for fluid particles, Int. J. Multiph. Flow. 15 (1989) 573–588. https://doi.org/10.1016/0301-9322(89)90054-2.

[188] G. Kelbaliyev, K. Ceylan, Estimation of the minimum stable drop sizes, break-up frequencies, and size distributions in turbulent dispersions, J. Dispers. Sci. Technol. 26 (2005) 487–494. https://doi.org/10.1081/DIS-200054602.

[189] L. Hagesaether, H.A. Jakobsen, H.F. Svendsen, A model for turbulent binary breakup of dispersed fluid particles, Chem. Eng. Sci. 57 (2002) 3251–3267. https://doi.org/10.1016/S0009-2509(02)00197-5.

[190] H. Luo, H.F. Svendsen, Theoretical Model for Drop and Bubble Breakup in Turbulent Dispersions, AIChE J. 42 (1996) 1225–1233. https://doi.org/10.1002/aic.690420505.

[191] C. Desnoyer, O. Masbernat, C. Gourdon, Experimental study of drop size distributions at high phase ratio in liquid-liquid dispersions, Chem. Eng. Sci. 58 (2003) 1353–1363. https://doi.org/10.1016/S0009-2509(02)00461-X.

[192] J.O. Hinze, Fundamentals of the hydrodynamic mechanism of splitting in dispersion processes, AIChE J. 1 (1955) 289–295. https://doi.org/10.1002/aic.690010303.

[193] G. Stiesch, Modeling Engine Spray and Combustion Processes, Springer, Berlin, 2003. https://www.springer.com/gp/book/9783540006824.

[194] M.H. Bordbar, T. Hyppänen, Modeling of binary collision between multisize viscoelastic spheres, J. Numer. Anal. Ind. Appl. Math. 2 (2007) 115–128.

[195] P. Zamankhan, M.H. Bordbar, Complex flow dynamics in dense granular flows - Part I: Experimentation, J. Appl. Mech. Trans. ASME. 73 (2006) 648–657. https://doi.org/10.1115/1.2165234.

[196] M.H. Bordbar, P. Zamankhan, Dynamical states of bubbling in vertical vibrated granular materials. Part II: Theoretical analysis and simulations, Commun. Nonlinear Sci. Numer. Simul. 12 (2007) 273–299. https://doi.org/10.1016/j.cnsns.2005.03.008.

[197] M.H. Bordbar, P. Zamankhan, Dynamical states of bubbling in vertically vibrated granular materials. Part I: Collective processes, Commun. Nonlinear Sci. Numer. Simul. 12 (2007) 254–272. https://doi.org/10.1016/j.cnsns.2005.04.001.

[198] P. O'Rourke, F. Bracco, Modeling of drop interactions in thick sprays and a comparison with experiments, in: Proc. Inst. Mech. Eng, 1980: pp. 101–116. https://scholar.google.com/scholar_lookup?hl=en&volume=9&publication_year=1980&pages=101-116&author=P.+O%27Rourke&author=F.+Bracco&title=Modeling+of+drop+interactions+in+thick+sprays+and+a+comparison+with+experiments.

[199] D.P. Schmidt, C.J. Rutland, A New Droplet Collision Algorithm, J. Comput. Phys. 164 (2000) 62–80. https://doi.org/10.1006/jcph.2000.6568.

[200] CD-ADAPCO, STAR CCM+ User Guide (Version4.02), (2008) 1–406.

[201] S. Kim, D.J. Lee, C.S. Lee, Modeling of binary droplet collisions for application to inter-impingement sprays, Int. J. Multiph. Flow. 35 (2009) 533–549. https://doi.org/10.1016/j.ijmultiphaseflow.2009.02.010.

[202] H. Zhang, Y. Li, J. Li, Q. Liu, Study on separation abilities of moisture separators based on droplet collision models, Nucl. Eng. Des. 325 (2017) 135–148. https://doi.org/10.1016/j.nucengdes.2017.09.030.

[203] C. Rabe, J. Malet, F. Feuillebois, Experimental investigation of water droplet binary collisions and description of outcomes with a symmetric Weber number, Phys. Fluids. 22 (2010) 1–11. https://doi.org/10.1063/1.3392768.

[204] P.R. Brazier-Smith, S.G. Jennings, J. Latham, The interaction of falling water drops: coalescence, Proc. R. Soc. London. A. Math. Phys. Sci. 326 (1972) 393 LP – 408. http://rspa.royalsocietypublishing.org/content/326/1566/393.abstract.

[205] N. Ashgriz, J.Y. Poo, Coalescence and separation in binary collisions of liquid drops, J. Fluid Mech. 221 (1990) 183–204. https://doi.org/10.1017/S0022112090003536.

[206] C. Hu, S. Xia, C. Li, G. Wu, Three-dimensional numerical investigation and modeling of binary alumina droplet collisions, Int. J. Heat Mass Transf. 113 (2017) 569–588. https://doi.org/10.1016/j.ijheatmasstransfer.2017.05.094.

[207] C.G. Sedano, C.A. Aguirre, A.B. Brizuela, An Eulerian-Lagrangian Coupled Model for Droplets Dispersion from Nozzle Spray, 2018. https://doi.org/10.5772/intechopen.81110.

[208] J. Wei, Y. Li, Enhanced spread of expiratory droplets by turbulence in a cough jet, Build. Environ. 93 (2015) 86–96. https://doi.org/10.1016/j.buildenv.2015.06.018.

Appendix I: Eulerian and Lagrangian approaches for multiphase flows

A1.1. Approaches for multiphase flow simulation

From a fluid mechanics point of view, cough and sneeze can be modeled as a turbulent jet [181,182] since the typical Reynolds number of these jets, calculated based on jet diameters, is higher than 5,000 [149,152]. The governing equations of a fluid flow have been developed from conservation laws, including mass, momentum, and energy conservation. Also, in an airborne droplet/particle field, the multiphase nature of the flow is modeled via one of the two main approaches, namely Eulerian and Lagrangian, as shown in Fig. A1.1. The main difference between the Eulerian and Lagrangian methods is related to their investigated frame of reference, which is fixed in the Eulerian methods while it is following a fluid element along its path-line in the Lagrangian one. The numerical procedure and algorithm of solution of Eulerian format of governing equations described in [183]
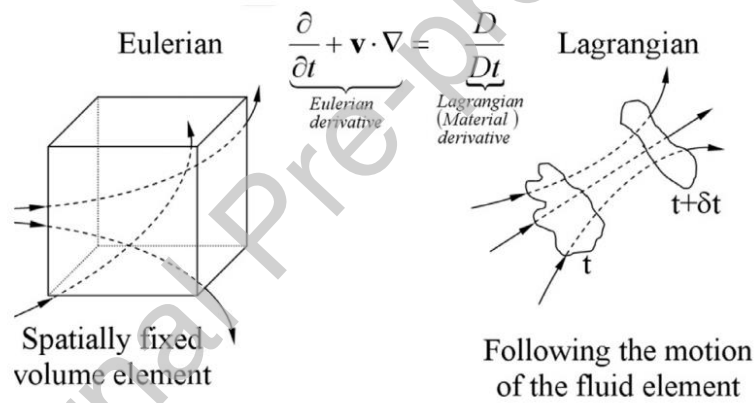
Fig. A1.1: Eulerian (left) and Lagrangian (right) approaches in fluid mechanics

A1.1.1. Eulerian models for multiphase flows

In the Eulerian approach (also known as Euler-Euler or multi-phase model), two or more phases of gas, fluid, or solid are treated as continuous phases. This means that all phases coexist everywhere in the domain while each phase's volumetric fraction is considered a continuous parameter in space and time. Thus, the conservation of mass, momentum, energy, and turbulence are solved for each phase in the Eulerian models. The most popular Eulerian models available for numerical simulations are Volume of Fraction (VOF), Mixture Model, and Eulerian Model [9]. These models are not capable of tracking discrete particles, and hence they are not detailed in the modeling of airborne pathogen droplets. Also, their unsteady time-step values are usually limited by grid size due to stability or accuracy [184].

A1.1.2. Lagrangian Models for multiphase flows

Lagrangian approaches, also known as Euler-Lagrange, simulate discrete particles as each particle can freely move through space and time within a continuous phase. The continuous phase is usually solved with Eulerian equations, while the discrete phases are coupled with Lagrangian equations. The coupling with the continuous fluid can be set to be one-way or two-way coupling [9]. In a complex situation, the continuous phase can be a mixture of fluids with different material properties. Also, particles can be solid materials or a mixture of solid-fluid or fluid-fluid with different properties and sizes. Hence, this approach is a promising method to model airborne pathogen droplets. In addition, it is possible to use the assumption of different forces such as drag, shear-induced lift gravity, etc., on the particles (depending upon the nature of the mixture). Furthermore, the energy equation can be taken into account in the calculations. Thus, droplet evaporation or collision can be included in the Lagrangian models. The discrete phase trajectory is calculated using a Lagrangian framework that includes the discrete phase inertia, hydrodynamic drag, and gravity force. Prediction of the effects of turbulence on the dispersion of particles due to turbulent eddies can be implemented in the continuous phase.

Comparing Euler-Lagrange and Euler-Euler methods, the former is computationally more expensive since the Lagrangian equations of motion applied to a 3-D domain are more complex in most applications [185]. Also, since Euler-Lagrange keeps tracking large numbers of particles in a flow field, it requires more computations and memory than the Euler-Euler method [184]. Nonetheless, the Lagrangian approach is diffusion-free and highly parallelizable as all particles are advected independently. In addition, the Lagrangian method is recognized to be CFL-free [186].

Appendix II: Different phenomena related to airborne pathogen transmission and dispersion

A2.1. Droplet Breakup

Droplet breakup is a complex phenomenon that is investigated through different criteria, including Kelvin-Helmholtz and Rayleigh-Taylor instability theory. As a result, the break-up of a droplet has two criteria, including the diameter of falling/rising droplet that cannot exceed a maximum diameter without break-up [187], and droplets with diameters smaller than a certain value should not break up [188]. In addition, it is generally accepted that turbulent breakage is the dominant mechanism in turbulent dispersions [189–192]. If the size of a drop (d) is larger than the maximum stable drop size (dS), then the drop first undergoes a shape deformation and then breaks up. For the droplets that are among those which can break up, the process is usually investigated via non-dimensional numbers.

Break-up occurs under the action of non-uniform surface forces. This is usually known as a secondary breakup. A droplet's reaction to non-uniform surface forces is invariably deform, and the deformation of the droplet is resisted by viscous forces inside the droplet and the surface tension. Droplets behavior to breakup phenomenon depends on the Weber and Ohnesorge numbers:

$$We = \rho_g |V_s|^2 D_p / \sigma \qquad (1)$$

$$Oh = \mu_l / \sqrt{\mu_l D_p \sigma} \qquad (2)$$

where, $\rho_g, V_s, D_p, \sigma,$ and μ_l represent the gas density, the particle slip velocity, the particle diameter, the surface tension of the droplet, and the viscosity of the liquid, respectively.

While detailed modeling of even one breakup regime is difficult, different breakup regimes have been identified, depending on the values of these forces. The purpose of the secondary breakup models is to predict when breakup occurs and what diameters can be resulted from it. In general, breakups are characterized by the shape of the deforming droplets [193], as shown in Fig. A2.1.

Fig. A2.1: Shape of particle breakdowns with respect to Weber number [193]

A2.2. Droplet Collision

While collision between solid particles [194,195] in many flow regimes such as dense fluidized beds is the most important mechanism in terms of the momentum and energy transfer within the system [196,197], in the two-phase flow of the respiratory droplets, the effect of particles collisions is not considered to be significant though still needs to be included especially if computational resources are sufficient

A2.2.1. Number of collisions

As a classical collision model, O'Rourke's [198] model calculates the droplets' collisions in a Lagrangian frame. This model assumes that droplets or particles are distributed uniformly in the cell, and only two particles that share the same cells may collide. The collision algorithm of O'Rourke is known as the standard approach, which has been widely used in spray simulations and has a computational cost proportional to the square of the number of computational particles or parcels [199].

The no-time-counter (NTC) method, mainly applied to gas dynamics simulations, has been used in cases with varying numbers of droplets per parcel. If a cell contains "N" droplets, the expected number of collisions in the cell over a time interval is given by summing the probability of all possible collisions:

$$M_{coll} = \frac{1}{2} \sum_{i=1}^{N_p} q_i \sum_{j=1}^{N_p} q_j \frac{v_{i,j} \sigma_{i,j\Delta t}}{V} \tag{3}$$

$$\sigma_{i,j} = \pi(r_i + r_j)^2 \tag{4}$$

where $v_{i,j}$ is the relative velocity between two colliding parcels, $\sigma_{i,j}$ is the collision cross-section of the two droplets, Δt is the time-step size, V is the cell volume, N_p is the number of parcels in a cell, and q_i is the number of droplets in the parcel. Equation 3 can be modified by pulling a constant factor outside:

$$M_{coll} = \frac{(qv\sigma)_{max}\Delta t}{2V} \sum_{i=1}^{N_p} q_i \sum_{j=1}^{N_p} q_j \frac{q_j v_{i,j}\sigma_{i,j}}{(qv\sigma)_{max}} \tag{5}$$

The value of $(qv\sigma)_{max}$ is used to scale the selection probability of a collision [9]. The NTC is much faster and slightly more accurate than O'Rourke's method. The NTC considers only a sample of collision pairs. However, it scales up the probability of collision so that each pair of collisions is more likely to be selected. According to the STARCCM user guide [200], the computational cost of NTC is linearly proportional to the number of particles (Np). On average, the result is similar to the modeling of a full distribution of particles. Fig. A2.2 demonstrates a comparison between the CPU costs of the NTC scheme and the O'Rourke's model.
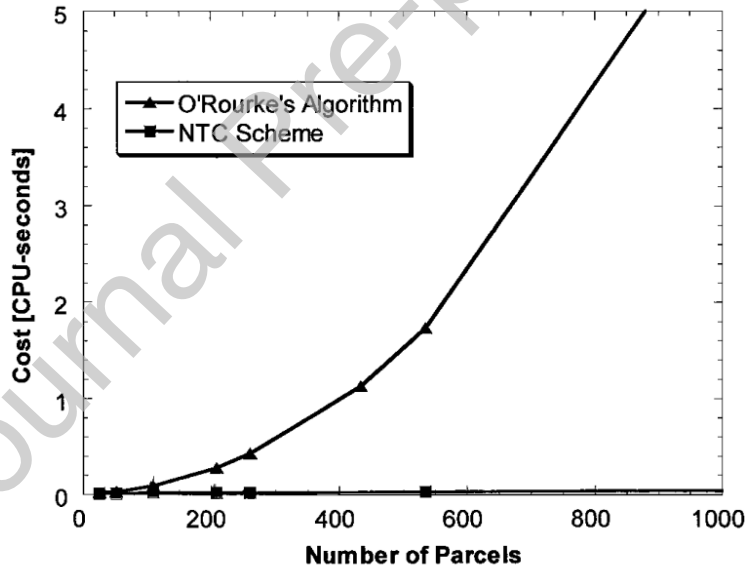

Fig. A2.2: Comparison between the computational costs of the NTC scheme [94] and the O′Rourke′s algorithm [93]

A2.2.2 Binary collision model for liquid droplets

This model is based on binary collision and is a widely used approximation for obtaining the final interaction between colliding droplets [121,201–206]. The model is used to estimate the positions, velocities, and diameters of the droplets after the collisions. Furthermore, the models can assume the

flying droplets (satellite droplets) from the ligament breakup. The binary droplet collision model is developed based on three parameters, including the ratio of the diameters of colliding droplets (Δ), the dimensionless symmetric Weber number (We) [203], and the dimensionless impact parameter used to include how the colliding droplets hit each other::

$$\Delta = \emptyset_s / \emptyset_L \tag{6}$$

$$We = \frac{\rho_l \emptyset_s \Delta^3 |\vec{V}_{mS}|^2 + |\vec{V}_{mL}|^2}{12\sigma\Delta(1 + \Delta^2)} \tag{7}$$

$$Imp = \frac{2X}{\emptyset_s + \emptyset_L} \tag{8}$$

where the subscripts *L* and *S* represent the larger and smaller droplets, respectively. In addition, $\emptyset$ is the droplet diameter, ρ_l symbolizes the liquid particles' density, σ is the surface tension, and $\vec{V}_{mL}$ and $\vec{V}_{mS}$ are the vector of the relative velocities of the mass centers of the colliding droplets. Finally, X represents the projected distance between droplets centers in the normal direction to the relative velocity vector.

In general, Fig. A2.3 demonstrates four distinguishable collision scenarios:

1- Coalescence (C): It is the process where the two colliding droplets form a single drop. This happens when the surface energy is relatively larger than the kinetic energy.

2- Reflexive (R): The two colliding droplets collide in the normal direction (head-on), forming a single droplet. Here, the kinetic energy is large enough to separate again and generate satellite droplets.

3- Stretching (S): the two drops collide tangentially. Thus, after the collision, they separate again and generate satellite droplets.

4- Bouncing (B): no mass exchanging occurs after a collision of two droplets, and they may remain separated after the collision.
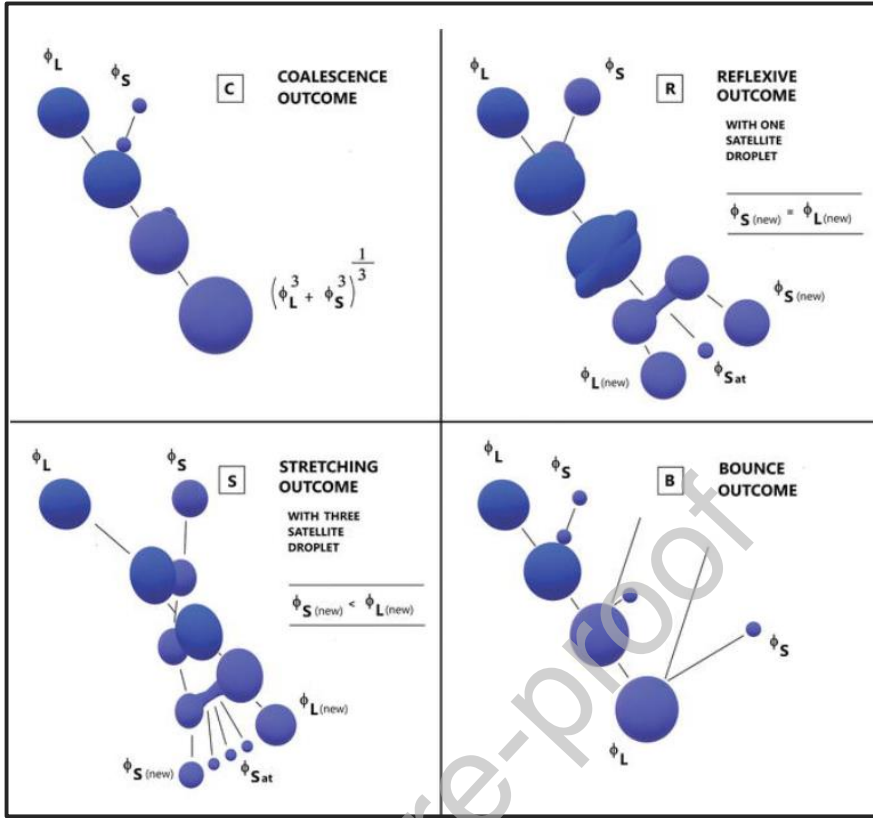
Fig. A2.3: Different scenarios of droplet collisions (Map: Coalescence (C), Reflexive (R), Stretching (S), and Bouncing (B)). [207]

A2.3. Droplet Evaporation

Respiratory droplets are usually either pure water droplets or non-evaporative nuclei (such as viruses or mucus) covered with an evaporative surface. Thus, after being released from a bio-source, their water-based outer crusts start to evaporate. The final size, mass, and consequently the airborne behavior of the remaining (non-evaporative) parts of the droplets depend on evaporation. Small droplets tend to evaporate very quickly [14, 96]. Wei and Li [208] employed the following equation for modeling an evaporation process:

$$\frac{dm_p}{dt} = \frac{2\pi P d_p M_w D_\infty C_T \, Sh}{RT_\infty} ln\left(\frac{P - P_{vs}}{P - P_{v\infty}}\right) \tag{9}$$

where P is total pressure, d_p denotes particle diameter, M_w is the molecular weight of water vapor, D_∞ is the binary diffusion coefficient far from the droplet, C_T is the correctional factor, R is the universal gas constant, T_∞ is the temperature, P_{vs} the vapor pressure at the droplet surface, and $P_{v\infty}$ is the vapor pressure distant from it. Sh denotes the Sherwood number and accounts for the enhanced mass transfer rate by convective effect and is defined as:

$$Sh = 1 + 0.38 Re^{0.5} Sc^{0.3334} \tag{10}$$

where Sc is the Schmidt number of the continuous phase, and is defined as the ratio of momentum diffusivity (kinematic viscosity) and mass diffusivity, and is used to characterize fluid flows in which there are simultaneous momentum and mass diffusion convection processes.

The C_T is calculated as:

$$C_T = \frac{T_\infty - T_P}{T_\infty^{\lambda-1}} - \frac{2-\lambda}{T_\infty^{2-\lambda} - T_p^{2-\lambda}} \tag{11}$$

λ (a constant between 1.6 and 2.0) is the correction factor due to the diffusion-coefficient temperature dependency.

Finally, the equation of heat transfer through the droplet surface can be explained as:

$$\left(m_{p,l}C_l + m_{p,s}C_s\right)\frac{dT_p}{dt} = \pi d_p^2 K_g \frac{T_\infty - T_p}{r_p} Nu + L_v \frac{dm_p}{dt} \tag{12}$$

where $m_{p,s}$ and $m_{p,l}$ are the solid and liquid mass of the particle, Nu is the Nusselt number as given by Nu=1+0.36Re$^{0.5}$ Pr$^{0.33}$, C_l and C_s are the specific heat transfer of pure water, and 1000 J/(kg.K), K_g is the thermal conductivity of air, and L_v is the latent heat of vaporization.

Redrow et al. [137] presented a modified evaporation model for multi-component droplets to simulate the behaviors of the viral-laden sputum droplets. This model included the effects of droplet velocity, ambient humidity, and temperature, as well as chemical components and surface tension. Consequently, the rate of change of droplet radius can be estimated by:

$$r_p \frac{dr_p}{dt} = \frac{D_v M_w P_{sat}}{\rho_s R T_a} \left\{ RH - \frac{1}{1+\delta} exp\left[A + B - C\sum_i \frac{I_i O_i y_i}{M_i}\right] \right\} \tag{13}$$

Coefficients A, B, and C are defined as:

$$A = \frac{L_v M_w}{R T_a}\left(\frac{\delta}{1+\delta}\right) \tag{14-a}$$

$$B = \frac{2M_w \sigma_s}{R T_a (1+\delta) r \rho_w}, \tag{14-b}$$

$$C = \frac{M_w \rho_N r_N^3}{(r^3 + r_N^3)\rho_w} \tag{14-c}$$

where $\delta = \frac{T_p}{T_a} - 1$. $I_i, O_i, and\ y_i$ are the number of ions into which a solute molecule dissociates, the practical osmotic coefficient, and the mass fraction of constituent i, respectively. In addition, subscript N refers to the dry particle, and σ is the surface tension. RH is the relative humidity and P_{sat} is the saturation vapor pressure given by:

$$P_{sat} = 6.1121(1.0007 + 3.46 \times 10^{-6}P)exp\left(\frac{17.502 T_a}{240.97 + T_a}\right) \tag{15}$$

In a more recent study by Li et al. [136], an evaporation model is introduced as a function of diffusion mechanism and the mass transfer rate calculated through the below equation:

$$\frac{dm_p}{dt} = -\pi d_p D_v Sh \frac{M_v}{M_a} ln\left(\frac{1 - X_{v,s}}{1 - X_{v,mix}}\right) - \pi d_p D_v Sh \frac{M_v}{M_a} ln\left(\frac{P - P_{v,p}}{P - P_v}\right) \tag{16}$$

The evaporation of water in a droplet is controlled by the equilibrium vapor pressure at the droplet surface relative to the ambient pressure. By considering the effect of non-volatile part dispensable, the equilibrium vapor pressure at the droplet surface, $P_{v,p}$, is calculated as:

$$P_{v,p} = P_{scale}\, e^{\left(12.430 - \frac{4233.7}{T_d + -31.737}\right)} \tag{17}$$

where P_{scale}=1.0 bar. The evaporation model of Eq. (15) was also exploited by Yan et al. in 2019 to study the influence of the thermal aspect of a human body on the transient dispersion of cough droplets considering evaporation [6].